

Project Number: CF – VX17

# **Vortex Tube Cooling System**

A Major Qualifying Project Report

Submitted to the Faculty

of the

WORCESTER POLYTECHNIC INSTITUTE

In partial fulfillment of the requirements for the  
Degree of Bachelor of Science in Mechanical Engineering

By

---

Devin J. Duarte

---

Kimberly R. Rosa

---

Daniel A. Ruiz-Cadalso

Date: 1 May, 2017

Keywords:

1. Vortex Tube
2. Cold fraction
3. Chamber

---

Professor Cosme Furlong-Vazquez

## **Abstract**

All of the technologies we rely on, from smartphones to laptops, are powered by semiconductor computer chips that continue to innovate in the miniaturization of their features. Smaller features lead to smaller tolerances in manufacturing, meaning that uniform and rapidly adaptable cooling is increasingly indispensable to the photolithography process. This project evaluated the use of a vortex tube for cooling the photolithography machines used in semiconductor manufacturing for ASML. This technology is not traditionally used in this setting, but is more adaptable and efficient than current solutions and provides an opportunity for innovation in this vital industry. Theoretical, computational, and experimental methods were developed to quantitatively study the feasibility of using the vortex tube in this application. Experiments were conducted in an environment designed and fabricated by the team to simulate the chip manufacturing process. The vortex tube, with some future work and adjustments, was found to be a viable alternative to current cooling systems.

## **Acknowledgements**

We would like to thank our project advisor, Professor Cosme Furlong-Vazquez, for his guidance and support throughout the entire project process. His expertise was essential in many aspects, and helped us find the right direction for our project, which was vital to its success.

We would like to thank the Center for Holographic Studies and Laser micro-mechaTronics (CHSLT) at Worcester Polytechnic Institute for allowing us to use their facilities for experimentation and providing their support to our project, specifically Haimi Tang, Payam Razavi, and Koohyar Pooladvand, among others. Our thanks are also with the staff in the Mechanical Engineering department at Worcester Polytechnic Institute, whose support and guidance was invaluable, specifically lab manager Peter Hefti and Barbara Furhman.

Finally, thank you to our sponsor, ASML, for their funding and support for our project. Specifically, thanks to ASML engineers, Andy Judge, Santiago Delpuerto, Claire Chen, Lowell Baker, and Ryan Maidhof for allowing us to gain a unique insight into real-life engineering in industry during the project experience.

## **Authorship**

All team members contributed equally to this project.

## TABLE OF CONTENTS

Abstract	ii
Acknowledgements	iii
Authorship	iv
Table of contents	v
List of figures	viii
List of tables	xi
Nomenclature	xii
Objective	xiv
Project statement	xv
1. Introduction and background	1
1.1. Vortex tube	3
1.1.1. History	3
1.1.2. Description	3
1.1.3. Commercial vortex tubes	4
1.1.3.1. Size	4
1.1.3.2. Cooling capacities	5
1.1.3.3. Performance charts	5
1.1.4. General equations and terms	7
1.1.5. Energy separation	11
1.1.5.1. Velocity, temperature and pressure distributions	12
1.1.5.2. Temperature separation	16
1.1.6. Vortex fluid flow	17
1.2. Flow-induced vibrations	18
1.3. Thermofluids physics	20
1.3.1. Fluid mechanics of flow over flat plate	20
1.3.2. Forced convection over flat plate	21
1.4. Clean room requirements	23
2. General methodologies	24
3. Project schedule and tasks	26
4. Theoretical development methods	27
4.1. Parametric analysis on vortex tube	27
4.2. Thermofluids analysis of vortex tube flow over flat plate	30

4.2.1. Velocity and boundary layer thickness profiles	31
4.2.2. Lumped capacitance for transient heat dissipation	33
5. Computational simulation methods	36
6. Experimental methods of a vortex tube's capabilities and limits	37
6.1. Design of experiments	37
6.2. Design of experimental setup	38
6.3. Experimental procedures	41
6.4. Data acquisition logic process	42
7. Experimental methods of a vortex tube's integration in the designed chamber	44
7.1. Design of experiments	44
7.2. Design of experimental setup	44
7.3. Experimental procedures	46
8. Facilities and instrumentation	47
8.1. Chamber construction	48
8.2. Monitoring Instrumentation	50
9. Results and discussions	52
9.1. Computational and theoretical comparisons	52
9.2. Experimental results of a vortex tube's capabilities and limits	53
9.2.1. Cold fraction variations	56
9.2.2. Input pressure variations	57
9.2.3. Reduction of overall thermal time constants	58
9.3. Experimental results from forced convection cooling of a heated plate	60
9.3.1. Temperature distributions from IR thermal imaging	62
9.3.2. Thermocouple temperature data plotted over time	64
10. Conclusions	67
10.1. Experimental results of a vortex tube's capabilities and limits	67
10.2. Reduction of overall thermal time constants	67
10.3. Experimental results from forced convection cooling of a heated plate	68
10.4. Temperature distributions from IR thermal imaging	69
10.5. Thermocouple temperature data plotted over time	69
11. Future work and recommendations	70
References	71
APPENDIX A. Project schedule in Gantt chart form	72
APPENDIX B. Derivation of velocity distribution function over flat plate	73
APPENDIX C. Detailed steps on modelling turbulence for simulation of flow over plate	75

APPENDIX D. LabVIEW VI data acquisition coding	78
APPENDIX E. List of instrumentation and apparatus	85

## List of Figures

Fig. 1.	Schematic Representation of the Vortex Process inside the Vortex Tube	4
Fig. 2.	Schematic drawing of the velocity distribution and trajectory throughout the tube	13
Fig. 3.	Control surface for lumped capacitance analysis (Cengel et. al, 2014)	22
Fig. 4.	Design process flowchart	24
Fig. 5.	Established control systems for facilitation of analyses	25
Fig. 6.	Temperatures at cold outlet with varying cold fractions and input pressures	28
Fig. 7.	Reynold's number for various input pressures, input mass flow rates and cold fractions	30
Fig. 8.	Schematic representation of fluid exhaustion flow from the nozzle over the flat plate	31
Fig. 9.	Boundary layer plotted over plate length for various flows	33
Fig. 10.	Schematic representation of heat transfers in the plate	34
Fig. 11.	Surface temperature of the plate for various cooling flow temperatures over time	35
Fig. 12.	Expanded tree manager and geometry after modelling the simulation in COMSOL	36
Fig. 13.	Vortex tube experimental setup block diagram	39
Fig. 14.	Schematic diagram of the developed experimental setup for vortex tube testing	40
Fig. 15.	SolidWorks CAD model of the setup (a) at the vortex tube, and (b) at the accumulator	41
Fig. 16.	Schematic diagram of the developed experimental setup for chamber testing	45
Fig. 17.	Chamber CAD designed in SolidWorks	45
Fig. 18.	Picture of assembled setup at the provided facility	47
Fig. 19.	Assembled chamber frame with welded acrylic sheets	48

Fig. 20. Assembling of the chamber with instrumentation	49
Fig. 21. Constructed chamber for experimentation	49
Fig. 22. Omega FMA1000-R V1 air velocity/temperature transmitter	50
Fig. 23. Omega PX-181B-100G5V pressure transducer	51
Fig. 24. Infrared camera FLIR SC6000 series (FLIR)	51
Fig. 25. Velocity (m/s) contour plot with rainbow color scale in COMSOL	52
Fig. 26. Comparison of COMSOL streamline velocity data to theoretical model	53
Fig. 27. Experimental setup showing accumulator, pressure regulators and monitoring sensors	54
Fig. 28. Experimental setup consisting of a vortex tube, DAQ box, and monitoring sensors	55
Fig. 29. Cold temperatures plotted over time for varying cold fractions	56
Fig. 30. Cold temperatures plotted over time for varying input pressures	57
Fig. 31. Cold temperatures plotted over time for the forced experiment	59
Fig. 32. Thermocouple placements throughout the plate	61
Fig. 33. Positioning for infrared camera to capture area of interest	62
Fig. 34. Thermal imaging of forced convection from IR camera	63
Fig. 35. Temperature data for all thermocouples during heating and cooling experiments	65
Fig. 36. Temperature data from the first thermocouple plotter over time	66
Fig. 37. Project schedule in Gantt chart form	72
Fig. 38. Turbulent flow, $k-\epsilon$ physics settings in COMSOL	75
Fig. 39. Boundary conditions chosen as wall functions (blue lines) in COMSOL	76
Fig. 40. Generated mesh of the air domain in COMSOL	77
Fig. 41. LabVIEW thermocouple read function	79

Fig. 42. LabVIEW analog input read function	80
Fig. 43. LabVIEW thermocouple conversion	81
Fig. 44. LabVIEW array function for sensor data	81
Fig. 45. LabVIEW velocity readings	82
Fig. 46. LabVIEW timing module	83
Fig. 47. LabVIEW write-to-spreadsheet function	84

## **List of tables**

Table 1. EXAIR 3200 Series Vortex Tube Specifications	5
Table 2. Arizona Vortex Tube Manufacturing Company Performance Chart	7
Table 3. Dimensionless Analysis Data for Flow-Induced Vibrations	20
Table 4. Curve fitted log functions for medium vortex tube cold fractions	27
Table 5. Designed experiments for vortex tube performance testing	38
Table 6. Detailed list of instrumentation and apparatus	85

## Nomenclature

$A_{Cross}$ ,	area of cross-section of tube ;	$h_s$ ,	enthalpy of air for isentropic conditions ;
$\epsilon$ ,	coefficient of eddy diffusion ;	$\dot{S}_t$ ,	entropy production rate ;
$\epsilon_h$ ,	coefficient of eddy diffusion for heat transfer ;	$\Psi$ ,	fluid mode shape function ;
$COP_{cr}$ ,	coefficient of performance ;	$f$ ,	friction factor ;
$\epsilon$ ,	cold mass fraction ;	$H$ ,	head ;
$\lambda, \zeta, b, c$ ,	constants of vibrational analysis ;	$\dot{Q}_H$ ,	heating capacity/power ;
$\dot{Q}_C$ ,	cooling capacity/power ;	$z$ ,	height ;
$\delta$ ,	deflection of tube ;	$[I_M]$ ,	Identity matrix ;
$\rho$ ,	density of air ;	$\kappa$ ,	Kármán's constant ;
$D_C$ ,	diameter at cold outlet ;	$\mu$ ,	kinematic viscosity ;
$D_0$ ,	diameter at inlet ;	$L_p$ ,	level of sound pressure ;
$\beta$ ,	diameter ratio, $D_C/D_0$ ;	$\dot{m}_C$ ,	mass flow rate at cold outlet ;
$\omega'$ ,	dimensionless angular velocity, $\omega/\omega_i$ ;	$\dot{m}_H$ ,	mass flow rate at hot outlet ;
$\Omega$ ,	dimensionless frequency ;	$m_T$ ,	mass of total, $m_{tube} + \rho A_{cross}$ ;
$r'$ ,	dimensionless radial distance, $r/r_i$ ;	$m_{tube}$ ,	mass of tube ;
$\mathcal{U}$ ,	dimensionless velocity parameter ;	$B$ ,	mass ratio, $\rho A_{cross}/m_T$ ;
$\eta_{is}$ ,	efficiency of isentropic conditions ;	$I$ ,	moment of inertia of tube ;
$\eta_W$ ,	efficiency-theoretical for a vortex tube ;	$p_{atm}$ ,	pressure at atmosphere ;
$E$ ,	Elastic Modulus of tube ;	$p_0$ ,	pressure at inlet ;
$h_C$ ,	enthalpy of air at cold outlet ;	$p_{ref}$ ,	pressure of reference ;
$h_0$ ,	enthalpy of air at inlet ;	$r_i$ ,	radius at interference ;

$r_{Outer}$ ,	radius at the inside wall of the tube ;	$u$ ,	velocity-radial ;
$r_R$ ,	radius where the mean velocity of the fluid is 0 due the wall friction ;	$u_i$ ,	velocity-radial at interference radius ;
$Re_i$ ,	Reynold's number at interference radius ;	$u_{Outer}$ ,	velocity-radial at outer radius ;
$Re_{Outer}$ ,	Reynold's number at outer radius of the outer vortex ;		
$\tau_w$ ,	shear stress at wall ;		
$R_m$ ,	specific gas constant ;	$C$ ,	pertaining to the cold outlet ;
$c_p$ ,	specific heat for constant pressure ;	$H$ ,	pertaining to the hot outlet ;
$\gamma$ ,	specific heat ratio, $c_p/c_v$ ;	$0$ ,	pertaining to the inlet ;
$[K]$ ,	stiffness matrix ;	$Outer$ ,	pertaining to hot vortex radius reference;
$T_C$ ,	temperature at cold outlet ;	$i$ ,	pertaining to the interference between the hot and cold vortices ;
$T_H$ ,	temperature at hot outlet ;	$l$ ,	loss ;
$T_0$ ,	temperature at inlet ;		
$T_s$ ,	temperature for isentropic conditions ;		
$T_S$ ,	temperature-static ;		
$k$ ,	thermal conductivity ;		
$t$ ,	time ;		
$v^*$ ,	velocity just outside the no-slip condition boundary ;		
$\omega$ ,	velocity-angular ;		
$\omega_{Outer}$ ,	velocity-angular at outer radius ;		
$v$ ,	velocity-axial ;		
$v_m$ ,	velocity-mean of the fluid ;		

**Subscripts**

## **Objective**

The objective of this project is to design a new cooling system for ASML that meets their specified requirements. The project's goal is to, by considering ASML's standards and system requirements, design and develop a cooling system using a vortex tube that completely fits their requirements and provides the following:

- Uniformly distributed temperature throughout the surface of the plate
- Relatively fast temperature adjustability (low Thermal Time Constant)
- Consistent and low-maintenance cooling system for ASML's photolithography machines

## **Project statement**

ASML is a Dutch company that manufactures photolithography machines for the production of microprocessors. They are among the leading suppliers of photolithography systems for semiconductor manufacturing companies in the world, such as Intel and AMD. Current semiconductor technology manufactures at the nanoscale. One such machine that ASML produces, the NXE, has extremely tight manufacturing tolerances, due to the highly precise nature of its photolithography process. The NXE's tolerance is in terms of nanometers, it “[offers] 22 nm resolution with conventional illumination and 18 nm with off-axis illumination” (ASML). Due to the NXE's use of EUV lasers, the silicon wafers undergo thermal expansion, which becomes a critical concern for the laser's precision. Standard silicon wafers can expand significantly if the temperature in the system fluctuates. This thermal expansion can cause inaccuracies in the resulting product, therefore ASML has provided an effective thermal management system to avoid this. ASML discovered a cooling technology, the vortex tube, that could potentially innovate the current cooling system process. However, the vortex tube was relatively untested for this particular application. Therefore, WPI and ASML partnered to explore the feasibility of using the vortex tube for thermal management. To be a feasible device for this application, the vortex tube based cooling system must:

- Not need the use of electricity or recirculating cooling fluids
- Not require more than 5 Watts of heat sources.
- Be able to provide full control of temperature adjustability.
- Be cost effective relative to the reality of ASML's request.
- Generate minimal structure-born noise disturbances to the NXE's precision
- Fit the requirements of a clean-room environment.

- Deliver uniform cooling throughout the surface of the plate in the chamber ( $< 100$  mK)
- Maintain the average temperature in the plate at  $23 \pm 1$  °C.

## 1. Introduction and background

Photolithography is a process that is vital to how the world works today. The process of photolithography involves using a photosensitive layer to imprint a design or pattern onto another material. Microprocessors and computer chips use this process to imprint their layout onto a wafer to ensure assembly accuracy. Many large companies entrenched in innovation in the technology sector, use large-scale photolithography machines to complete this process. ASML, a Dutch company, is a manufacturer of such machines.

Due to the highly precise nature of photolithography, the processes, as well as the materials used to print on, are very delicate. Therefore, the working environment is highly susceptible to excess air particles and heating. The problem of clean air is resolved through their requirement that their large photolithography machines be contained in spaces that are to ISO cleanroom standards. While ASML's current cooling system for a specific area of the machine is functional for their needs, it doesn't provide the high degree of flexibility they desire. Therefore, ASML has partnered with WPI to have a team of students investigate an alternative cooling technology, the vortex tube.

The vortex tube is a cooling system with no moving parts or power requirement. The design and shape of the tube allows air entering into the tube at a designated velocity to create a vortex around the walls of the tube. This vortex then cools a stream of air that forms in the middle of it, thus creating a cold air outlet in the system. Much research has been done in determining how the vortex tube itself works. This abundant research makes the team's efforts to properly analyze the vortex tube as a viable cooling option that much simpler.

Some challenges faced in developing this system are related to ASML's requirements and desired outcomes. Their standard for high precision requires that this potential cooling system

have a high degree of adjustability, which relates to having a low thermal time constant in the system. ASML is also looking for temperature uniformity in the chamber the team is working to cool. Since the materials that their customers print onto are so sensitive to heat transfer, uniformity across the entire target cooling area is essential to producing usable product. The last of the desired outcomes is the necessity for providing the target area with a high degree of temperature stability, to within 100 mK. These three outcomes are of the utmost priority when developing this project.

The purpose of the project is to design an effective cooling system for ASML, utilizing vortex tube technology that meets ASML's requirements and standards. This project will be accomplished through several different stages. The first stage will consist of detailed, accurate analysis on how to cool the system to ASML's preferences using the vortex tube. By understanding the physics involved in the system and determining the optimal way to cool the chamber, the team will thus be able to design an effective system. Once all analysis has been completed, the next step will be to build and test the prototype cooling system to validate analysis. After testing has been completed, the team will utilize any insights gained from the experimental stage to make any modifications to the system design. With these stages complete, the team will be able to present ASML with a proof-of-concept design that meets all project goals.

## **1.1. Vortex tube**

### **1.1.1. History**

In 1928, a French physicist named George Ranque was working with a vortex pump and noticed how hot and cold airstreams were being exhausted separately by the pump. Ranque rapidly noticed how to use this odd phenomenon to his advantage, and therefore created a small business firm, to explore the possibilities of generating profit from a potential product that separates hot and cold air without the need of moving parts. The firm was unable to make this happen, and the vortex cooling method remained in the dark until a German physicist, Rudolph Hilsch, recognized the phenomenon and published a widely-read scientific paper on the vortex tube. Since then, the vortex tube has been used for a wide-variety of uses; but in the present day it is mostly used for spot cooling treatments.

### **1.1.2. Description**

The vortex tube is a spot-cooling device that separates pressurized air into hot and cold streams without the need of moving parts or electricity. The amount of cold and hot air exhaust can be controlled by a valve that is placed at the hot air outlet. The vortex tube is small, lightweight, durable and maintenance free. It may be used for many applications, such as cooling electronic controls, machining operations, soldered parts, gas samples, heat seals, environment chambers, etc.

In general, when compressed air is fed into the vortex tube, a plastic generator, consisting of millimeter-scaled nozzles in helical position, orients the air tangent to the tube to instantaneously form a vortex flow. At the end of the tube, a certain amount of the air is

exhausted, while the residual is reflected by the cold fraction valve. The reflected flow maintains its vortex-form, however, slightly smaller. The two vortices, travelling in opposite directions, create a vacuum at the center axis of the tube. The flow-induced vibrations by the turbulence of the flow trigger energy transfer from the inner to outer vortex, due to the vacuum. Thus, the outer vortex gains heat while the inner vortex is being cooled throughout the length of the tube, Fig. 1.

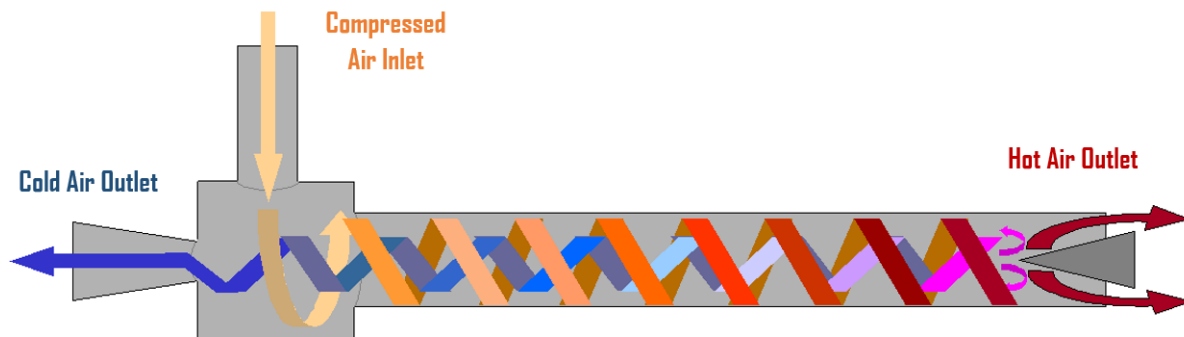


Fig. 1. Schematic Representation of the Vortex Process inside the Vortex Tube

### 1.1.3. Commercial vortex tubes

#### 1.1.3.1. Size

Some vortex tube manufacturers provide standard sizes with relatively wide ranges of cooling power. For example, EXAIR vortex tubes have the following three standard sizes: Small, 4.13” long; Medium, 5.68” long; and Large, 11.00” long. The Arizona Vortex Tube Manufacturing Company has two standard sizes for the tubes, 5.5” for the small one and 8.25” for the large one. Some manufacturers, however, will accept orders for custom-sized vortex tubes.

### 1.1.3.2. Cooling capacities

EXAIR Small vortex tubes can produce a range of 135 - 550 BTU/hour (161.2 Watts) of cooling power, while the Medium size can produce 650 - 2,800 BTU/hour (820.6 Watts) of cooling power, and the Large size can produce 3,400 - 10,200 BTU/hour (2989.3 Watts) of cooling power, Table 1.

Table 1. EXAIR 3200 Series Vortex Tube Specifications

Model #	SCFM*	SLPM*	BTU/hr**	Kcal/hr**	Size	dBa***
3202	2	57	135	34	Small	68
3204	4	113	275	69	Small	70
3208	8	227	550	139	Small	76
3210	10	283	650	164	Medium	80
3215	15	425	1000	252	Medium	81
3225	25	708	1700	428	Medium	82
3230	30	850	2000	504	Medium	84
3240	40	1133	2800	706	Medium	88
3250	50	1416	3400	857	Large	94
3275	75	2124	5100	1285	Large	96
3298	100	2832	6800	1714	Large	96
3299	150	4248	10200	2570	Large	97
* SCFM (SLPM) at 100 PSIG (6.9 bar) Inlet Pressure ** BTU/hr (Kcal/hr) Cooling Capacity at 100 PSIG (6.9 bar) *** Noise levels taken with hot and cold mufflers installed						

### 1.1.3.3. Performance charts

Most vortex tube manufacturers and suppliers provide a Performance Chart in their product data sheets. Most of these charts show a table relating pressure, temperature, and the

Cold Fraction. The Cold Fraction is the percentage of the volume of the exhaust cold air stream with respect to the inlet air consumption; in other words, the quantity of cold air that leaves divided by the quantity of air that is being fed to the system. These charts essentially explain that if the consumer wishes to reach a certain temperature with a certain cold air flow rate, then they must supply the vortex tube with the specified inlet pressure.

A certain characteristic about these performance charts is the relationship between cold fraction, temperature, and pressure. It is said the higher the cold fraction, the less the temperature drop one can achieve. In other words, if the consumer wants a higher flow rate at the cold air outlet, they would have to deal with a small temperature drop. However, if a relatively high temperature drop with a relatively high flow rate is required, then the inlet must be supplied with a higher pressure. See Table 2 for the Arizona Vortex Tube Manufacturing Company Performance Data.

Table 2. Arizona Vortex Tube Manufacturing Company Performance Chart

Inlet Pressure (PSIG)	Cold Fraction							
	°F	20 %	30 %	40 %	50 %	60 %	70 %	80 %
<b>20</b>	-ΔT	63.1	61.3	56.1	51.3	44.5	37	28.8
	+ΔT	15.1	24.4	37.8	51.3	65.1	82.5	108.1
<b>40</b>	-ΔT	89.2	85.8	81.1	73.2	63.1	52.5	39.1
	+ΔT	29.4	35.2	52.1	73.2	92.8	116.9	148.1
<b>60</b>	-ΔT	104.3	101.7	93.7	84.1	73.5	60.9	45.4
	+ΔT	25.6	39.9	59.1	84.1	104.1	133.1	169.1
<b>80</b>	-ΔT	117.1	111.2	102.3	92.2	81.3	66.2	50.1
	+ΔT	26.1	44.1	64.1	92.2	114.1	144.3	181.1
<b>100</b>	-ΔT	128.3	119.5	111.1	100.3	86.5	71.9	53.5
	+ΔT	27.8	46.1	67.3	100.3	119.9	151.1	192.1

#### 1.1.4. General equations and terms

An article called “A Review on Design Criteria for Vortex Tubes” (Yilmaz et. al, 2009) reviews basic terminology and equations simplified from basic Thermodynamics, Heat Transfer, and Fluid Mechanics theories. As mentioned, the cold flow-mass flow ratio is one of the most popular terms in vortex tube analyses. Since mass flow rates are essential in determining flow characteristics in a vortex tube, the cold mass ratio is exceedingly used because it facilitates calculations. With the aid of the cold mass ratio of a vortex tube, the inlet mass flow rate can be easily translated to outlet mass flow rates. The cold mass flow ratio (Yilmaz et. al, 2009) is determined as

$$\varepsilon = \dot{m}_c / \dot{m}_0 \quad . \quad (1.1)$$

$$1 - \varepsilon = \dot{m}_h / \dot{m}_0 \quad . \quad (1.2)$$

In the performance charts given by suppliers and manufacturers, for each cold flow mass ratio at a certain pressure, two quantities of temperature are given. The cold and hot temperature differences with respect to the inlet temperature (Yilmaz et. al, 2009) are

$$\Delta T_c = T_0 - T_c \quad . \quad (1.3)$$

$$\Delta T_h = T_h - T_0 \quad . \quad (1.4)$$

Additionally, a normalized cold and hot temperature drop and rise, respectively, are defined as the ratio of the temperature difference at their corresponding outlet with respect to the inlet temperature.

Furthermore, a parameter that may potentially influence the flow of the system as it leaves the vortex tube through the cold outlet is the cold outlet diameter. According to theories from fluid mechanics, the larger the diameter, the slower the fluid flow at a certain mass flow rate, and in turn, a lower Reynold's Number. A ratio that is used commonly in vortex tube analyses is the Cold Orifice Diameter Ratio,  $\beta$ , (Yilmaz et. al, 2009) , which is defined as

$$\beta = D_c / D_0 \quad . \quad (1.5)$$

In vortex tubes, like many other thermodynamically systems, the process is irreversible, and thus, not isentropic. Isentropic efficiencies will be present in this thermodynamic process, which is assumed to be isentropic expansion and not compression (Yilmaz et. al, 2009), and is defined as

$$\eta_{is} = \frac{h_0 - h_c}{h_0 - h_s} \quad . \quad (1.6)$$

For ideal gases, the specific heat at constant pressure is the same during the process, therefore, Eq. 1.6 simplifies to (Yilmaz et. al, 2009)

$$\eta_{is} = \frac{T_0 - T_c}{T_0 - T_s} \quad . \quad (1.7)$$

Thermodynamics will be reviewed in depth further in the Literature Review section, however, basic theories, terminology and equations can be seen here. Eq. 1.7 can be used for further simplification, for example, taking a look at the ideal gas law manipulated for isentropic processes, Eq. 1.8, which is

$$\frac{T_s}{T_0} = \left( \frac{p_c}{p_0} \right)^{\frac{\gamma-1}{\gamma}} \quad . \quad (1.8)$$

Thus, Eqs 1.7 and 1.8 can be combined (Yilmaz et. al, 2009) for defining the isentropic efficiency in terms of solely inlet and outlet parameters. This would be

$$\eta_{is} = \frac{T_0 - T_c}{T_0 \left[ 1 - \left( \frac{p_c}{p_0} \right)^{\frac{\gamma-1}{\gamma}} \right]} \quad . \quad (1.9)$$

Through relationships and theories, the pressure at the cold outlet was simplified in Eq. 1.9 in terms of atmospheric pressure, since it facilitates analysis and experimentation; the pressure at the cold outlet is not easily measured. Hilsch (Hilsch, 1947) developed his own definition for the thermodynamic efficiency of a vortex tube by comparing it to the cooling efficiency of a gas expanding adiabatically due to external work from an expansion engine. For adiabatic expansion of gas, the ideal gas is given isotropic conditions, where  $T_0/T_c = (p_0/p_c)^{(\gamma-1)/\gamma}$ . Meshing this with theories on heat removal of gas, and works due to expansion and compression, the efficiency of an expansion engine relying completely on inlet and outlet temperatures was derived. With this, by omitting the expansion work from the equation, it will be simplified to vortex tube conditions, which will result as a reliable vortex tube theoretical efficiency (Hilsch, 1947) determined by

$$\eta_W = \frac{x - 1}{x \ln x} , \quad (1.10)$$

where  $x = T_0/T_c$ .

Realistically in vortex tubes, there is work done by the system. However, this work is not easily calculated, and in most cases is negligible, since this is not one of the functions of the vortex tube. A PhD Thesis from Gao C. from Technische Universiteit Eindhoven called “Experimental study on the Ranque-Hilsch vortex tube” mentions and describes the coefficient of performance (COP) of a refrigerator, which is the ratio of cooling power over the working power, and translates it to determine a COP for the vortex tube as a refrigerator. The cooling power from the refrigerator is directly the cooling capacity from a vortex tube from the inlet to the cold outlet. The cooling capacity of the vortex tube can be defined as (Yilmaz et. al, 2009)

$$\dot{Q}_c = \dot{m}_c c_p (T_0 - T_c) . \quad (1.11)$$

Additionally, with Eq. 1.10 a formula for the COP of the vortex tube as a refrigerator was derived (Yilmaz et. al, 2009) to be

$$COP_{cr} = \frac{\gamma}{\gamma - 1} \frac{\varepsilon(T_0 - T_c)}{T_0 \ln\left(\frac{p_0}{p_c}\right)} . \quad (1.12)$$

Similarly, a COP for the vortex tube as a heat pump can be derived for the heat produced at the hot outlet. The heating power for the system and the COP for the vortex tube as a heat pump can be defined as (Yilmaz et. al, 2009)

$$\dot{Q}_h = \dot{m}_h c_p (T_h - T_0) . \quad (1.13)$$

$$COP_{hp} = \frac{\gamma}{\gamma - 1} \frac{(1 - \varepsilon)(T_h - T_0)}{T_0 \ln\left(\frac{p_0}{p_c}\right)} . \quad (1.14)$$

With this, a simple balance equation can be developed with theoretical efficiency conditions as

$$\eta_W \dot{m}_0 h_0 = (\dot{m}_c h_c + \dot{m}_h h_h) \quad . \quad (1.15)$$

Since most processes are irreversible, it would be beneficial to quantify this irreversibility. Gao C. derived a parameter called the Irreversibility Parameter,  $\Theta_{ir}$ , which provides a very good visualization of the isentropic efficiency of the vortex tube. In his experimentation results, all parameters  $\Theta_{ir}$  were very high, indicating that isentropic efficiencies in vortex tubes are very low and highly irreversible (Yilmaz et. al, 2009), and are determined by

$$\Theta_{ir} = \frac{\dot{S}_l}{\dot{m}_0 R_m} = \frac{1}{\Gamma} \ln \left( \frac{T_h^{1-\varepsilon} T_c^\varepsilon}{T_0} \right) - \ln \left( \frac{p_h^{1-\varepsilon} p_c^\varepsilon}{p_0} \right) \quad , \quad (1.16)$$

where

$$\Gamma = (\gamma - 1)/\gamma \quad . \quad (1.17)$$

Eq. 1.16 can be simplified with the use of the ideal gas law for isentropic processes, for which the result is

$$\Theta_{ir} = \frac{1}{\Gamma} \ln \left( \frac{T_h^{1-\varepsilon} T_c^\varepsilon}{T_0} \right) - \ln \left( \frac{p_0}{p_{atm}} \right) \quad . \quad (1.18)$$

### 1.1.5. Energy separation

Energy separation is the foundation of the vortex tube. It is the separation of the airstreams and temperatures that lead to the production of cold and hot air exhausts. This phenomenon, called the Ranque-Hilsch Effect was first reported by Ranque and later investigated experimentally by Hilsch.

Deissler (Deissler et. al, 1960), and later Kurosaka (Kurosaka, 1982), arrived at the conclusion that turbulent flow is necessary in any vortex flow for the separation of energy process to occur. Kurosaka (Kurosaka, 1982) mentions that articles in the past have investigated the energy separation phenomenon, but have only vaguely stated that it is due to unsteadiness in

the vortex flow. His article “submit[s] that the acoustical streaming of the gas with swirl produces the Ranque-Hilsch effect: the radial separation of total temperature”. After solving for first and second order differential equations for various layers, in addition to the “inviscid” core, throughout the tube, Kurosaka (Kurosaka, 1982) concluded that acoustic streaming is indeed a great influence for the energy separation phenomenon.

Ranges of noise that can be produced by vortex tubes will be investigated and evaluated to verify whether they are a potential concern for photolithography processes. The main concern, though, related to noise is the structure-borne noise, rather than air-borne.

#### **1.1.5.1. Velocity, temperature and pressure distributions**

Deissler (Deissler et. al, 1960) performed analysis on velocity distributions throughout a turbulent vortex fluid flow, which in turn provided them with enough information to be able to analyze the temperature and pressure distributions. Velocity distributions for all three components of the airstream that is hauled down from the hot airstream to the cold airstream will be reviewed and used throughout the rest of the section for temperature and pressure distribution. Since this airstream is travelling in a swirl-type flow along the axis of the tube while being attracted to the center of the axis, this airstream has three velocity components, Fig. 2: radial velocity ( $u$ ), angular velocity ( $\omega$ ), and axial velocity ( $v$ ).

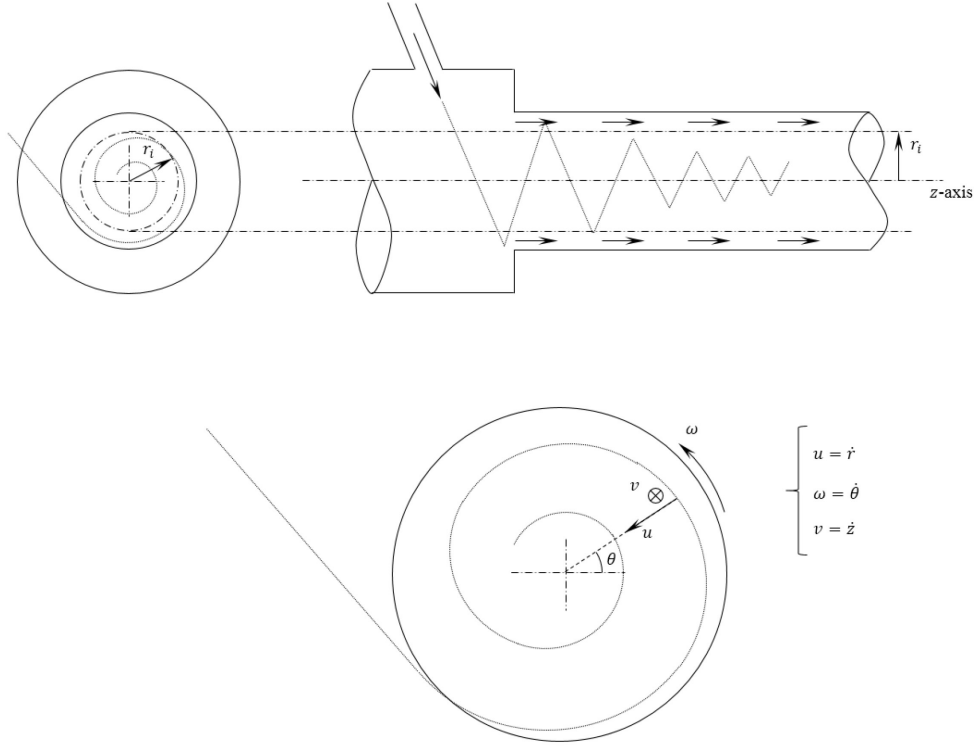


Fig. 2. Schematic drawing of the velocity distribution and trajectory throughout the tube

By the use of the compressible Navier-Stokes equation, a general solution for the angular velocity throughout the tube was determined. Keep in mind, however, that this velocity is not dependent of distance  $z$ , but of radius  $r$  (Deissler et. al, 1960). The solution is

$$\omega = \frac{c_1}{r} \int r e^{\int \frac{\rho u}{\rho \epsilon} dr} dr + \frac{c_2}{r} \quad , \quad (1.19)$$

where  $c_1$  and  $c_2$  are constants generated from differential analysis. By integrating the continuity equation  $[\partial(r\rho u)/\partial r + \partial(r\rho v)/\partial z = 0]$  to relate the axial flow to the radial flow, a very simple equation stands (Deissler et. al, 1960), and this is

$$r\rho u = - \int_0^r \frac{\partial(\rho v)}{\partial z} dr \quad . \quad (1.20)$$

Afterwards, considering the term  $\rho v$  has a step change at the interference between the two vortices, the definition of the angular velocity in dimensionless form becomes one dependent

on only the dimensionless radius  $r'$  and Reynold's number at the radius where the two vortices meet (Deissler et. al, 1960), and is defined as

$$\omega' = \frac{1}{r'} \left[ \frac{1 - \exp\left(-\frac{Re_i r'^2}{2}\right)}{1 - \exp\left(-\frac{Re_i}{2}\right)} \right] , \quad (1.21)$$

where

$$Re_i = \frac{\rho_i u_i r_i}{\rho \epsilon} . \quad (1.22)$$

These will become critical information for being able to correctly design geometrical and material properties of the vortex tube. If a newly-designed vortex tube becomes a project goal, it will have to be able to withstand these pressure and temperature distributions. The pressure caused by these vortex flows as they travel along the tube will generate vibrations, and in turn, fatigue. The potential newly-designed vortex tube will be designed to reduce these vibrations, and to withstand fatigue.

The steady-state energy balance equation for a compressible, axially asymmetric flow of a gas was simplified neglecting squares and products of very small quantities, adding three momentum equations to eliminate pressure gradients, and by assuming that the static temperatures ( $t$ ), the radial velocities, and the angular velocities are independent of the distance along the axial coordinate (Deissler et. al, 1960), and are determined by

$$c_p \rho u r \frac{\partial t}{\partial r} + r \rho u \frac{\partial (\omega^2/2)}{\partial r} - k \frac{\partial \left( r \frac{\partial T_s}{\partial r} \right)}{\partial r} = \mu \frac{\partial}{\partial r} \left\{ r \omega \left( \frac{\partial \omega}{\partial r} - \frac{\omega}{r} \right) \right\} . \quad (1.23)$$

They mention that, for large viscosities, that is, laminar flows with low radial velocities, the static temperature proves itself as constant. In other words, the static temperature throughout the tube is uniform due to conduction. However, for large radial flow (turbulent flow, low viscosity) the total temperature is uniform (Deissler et. al, 1960), and is

$$T_S + c_p \frac{v^2}{2} = \text{constant} \quad . \quad (1.24)$$

The energy equation was then simplified again, but for turbulent flows only, by adding eddy motion conditions. The eddy motion is the swirl of a fluid as it passes an obstacle. This type of fluid flow creates a diffusion process called the eddy diffusion, for which the parameter eddy diffusion coefficient,  $\epsilon$ , is introduced. The viscosity of the liquid and the thermal conductivity can be written in terms of the eddy diffusion coefficient for momentum ( $\epsilon$ ) and heat transfer ( $\epsilon_h$ ), respectively, which would simplify the energy balance equation to turbulent conditions (Deissler et. al, 1960) to

$$\begin{aligned} c_p \rho u r \frac{\partial T_S}{\partial r} + \frac{r \rho u}{2} \frac{d\omega^2}{dr} \\ = \frac{d}{dr} \left[ r \left\{ \rho c_p \epsilon \left( \frac{dT_S}{dr} - \frac{1}{\rho c_p} \frac{dp}{dr} \right) \right\} \right] + \frac{d}{dr} \left\{ \rho \epsilon r \omega \left( \frac{d\omega}{dr} - \frac{\omega}{r} \right) \right\} \quad , \end{aligned} \quad (1.25)$$

where

$$\mu = \rho \epsilon \quad , \quad (1.26)$$

and

$$k = \rho c_p \epsilon_h \quad . \quad (1.27)$$

Following conditions for isentropic expansion and contraction of eddies, the temperature distribution in this case should be isentropic rather than isothermal, and thus, this should simplify the relationship between temperature and pressure throughout the axis (Deissler et. al, 1960) to

$$T_S = \text{const.} p^\Gamma \quad , \quad (1.28)$$

or

$$\frac{dT_S}{dr} = \frac{1}{\rho c_p} \frac{dp}{dr} \quad . \quad (1.29)$$

Applying these analyses to the vortex tube specifically, Deissler (Deissler et. al, 1960) were able to analyze radially-distributed temperatures. They obtained an equation, for adiabatic tube and constant specific heat of air, to describe the temperature at the outer radius of the vortex flow in terms of inlet and outlet parameters (Deissler et. al, 1960), which is

$$T_0 - T_{Outer} = \frac{\dot{m}_c}{\dot{m}_0} (T_c - T_{Outer}) + \left(1 - \frac{\dot{m}_c}{\dot{m}_0}\right) (T_h - T_{Outer}) \quad . \quad (1.30)$$

### 1.1.5.2. Temperature separation

A study by Stephan (Stephan et. al, 1983) investigated the phenomenon, and through dimensional analyses they developed a similarity relation of the variation for the cold outlet temperature as a function of the cold mass ratio (Stephan et. al, 1983), which is

$$\frac{\Delta T_c}{\Delta T_{c,max}} = g(\varepsilon) \quad , \quad (1.31)$$

where

$$\Delta T_c = T_0 - T_c \quad , \quad (1.32)$$

$$\Delta T_{c,max} = T_0 - T_{c,max} \quad , \quad (1.33)$$

and

$$g(\varepsilon) = 0.792 + 1.540\varepsilon - 0.3101\varepsilon^2 + 0.815\varepsilon^3 \quad . \quad (1.34)$$

This similarity relation holds true for any vortex tube sharing similar geometry, and was confirmed and validated by their own experimentation analysis. In the Eqs 1.31-1.33,  $T_c$  is the temperature at the cold outlet. However, through the dimensional analysis dimensionless parameters were determined as functions of the independent parameters. Their experimental results indicated that if these dimensionless parameters were kept constant while the cold mass ratio  $\varepsilon$  approximated 1, the temperature at the cold outlet was possessing a maximum value, to

which  $T_{c,max}$  was introduced for. This similarity relation can be used “for predicting the temperature of the cold air of geometrically similar vortex tubes”.

### 1.1.6. Vortex fluid flow

Diessler (Deissler et. al, 1960), and later in Section 2.10 by Kurosaka [8], arrived at the conclusion that turbulent flow is necessary in any vortex flow for the separation of energy process to occur. This is explained later in detail in Section 2.10. Knowing this, Reynold’s number became an important factor in designing vortex flows and the energy separation aspects. By use of dimensional analysis, the eddy diffusion coefficient was estimated and related to the Kármán expression for the case of rectilinear flow. The eddy diffusion coefficient, in terms of the Kármán expression, becomes a constant for the outer vortex flow, and subsequently, facilitates the definition for the Reynold’s number that is based on the outer radius (Deissler et. al, 1960), and can be determined by

$$\epsilon = \kappa^2 \omega_{Outer} r_{Outer} / 2 \quad , \quad (1.35)$$

and

$$Re_{Outer} = - \frac{2 u_{Outer}}{\kappa^2 \omega_{Outer}} = \frac{1}{\epsilon} Re_i \quad , \quad (1.36)$$

where for flow through a tube or channel,  $\kappa$  ranges usually from 0.3 to 0.4. Keep in mind however, this Reynold’s number is based on the outer radius, and is equal to  $Re_i \dot{m}_0 / \dot{m}_C$ . Kármán’s constant is used to describe the flow of a fluid near a boundary with a no-slip condition, which is

$$v_m = \frac{v^*}{\kappa} \ln \left( \frac{r_{Outer} - r}{r_R} \right) \quad , \quad (1.37)$$

where

$$v^* = \sqrt{\frac{\tau_w}{\rho}} . \quad (1.38)$$

## 1.2. Flow-induced vibrations

ASML Photolithography processes are extremely precise, consisting of very small tolerances, and thus, vibrations by the vortex tube could generate structure-borne noise that can potentially disrupt this precision. This section investigates the vibrations induced by the vortex flow in the tube, and if said noise becomes a concern for the project, then a muffle/dampener device will be designed and constructed.

Blevins' Flow-Induced Vibration (Blevins, 1997) book dedicates a sub-section on fluid-flow-induced vibration in a cantilever pipe, which is the most similar situation to the vortex tube. As a general equation of motion for free vibration of a fluid-conveying pipe, the book determines one and makes use of it later throughout other sections (Blevins, 1997), which can be defined as

$$EI_x \frac{\partial^4 \delta}{\partial z^4} + \rho A_{cross} v^2 \frac{\partial^2 \delta}{\partial z^2} + 2\rho A_{cross} v \frac{\partial^2 \delta}{\partial z \partial t} + m_T \frac{\partial^2 \delta}{\partial t^2} = 0 , \quad (1.39)$$

where  $m_T = m_{tube} + \rho A_{cross}$  is the total mass (fluid and tube) per unit length. This equation meshed with a solution formula for the deflection of the cantilever tube results in a fourth-order differential equation consisting of the fluid mode shape function ( $\Psi$ ) and the dimensionless parameters  $B$ ,  $\Omega$ , and  $\mathcal{U}$ , followed by its solution (Blevins, 1997)

$$\Psi'''' + \mathcal{U}^2 \Psi'' + 2iB^{1/2} \mathcal{U} \Omega \Psi' - \Omega \Psi = 0 , \quad (1.40)$$

for which

$$B = \rho A_{cross}/m_T \quad , \quad (1.41)$$

$$\Omega = \omega_f L^2 \sqrt{m_T/EI} \quad , \quad (1.42)$$

and

$$\mathcal{U} = vL\sqrt{\rho A_{cross}/EI} \quad , \quad (1.43)$$

These dimensionless numbers have a great influence in natural frequencies of a pipe. For the cantilever pipe case, the most influential dimensionless number is the mass ratio  $B$ , a ratio of the fluid mass with respect to the total mass per unit of length. The dimensionless frequency  $\Omega$  is responsible for the production of vibrations on the cantilever tube. Belvins (Blevins, 1997) derived a matrix form solution for the dimensionless natural frequencies of the cantilever pipe system, which can be used to retrieve the nontrivial solutions of  $\Omega$  as a function of  $B$  and the dimensionless velocity parameter  $\mathcal{U}$ . This, in turn, provides solutions for vibrations in the tube generated by the fluid flow (Blevins, 1997), which is

$$|[K] - \Omega^2[I_M]| = 0 \quad , \quad (1.44)$$

where the entries of the stiffness matrix  $[K]$  are,

$$[K]_{nm} = \begin{cases} \lambda_m^4 + \mathcal{U}^2 c_{mn} + 2iB^{1/2}\mathcal{U}\Omega b_{mn} & ; m = n \\ \mathcal{U}^2 c_{mn} + 2iB^{1/2}\mathcal{U}\Omega b_{mn} & ; m \neq n \end{cases} \quad , \quad (1.45)$$

$$b_{nm} = \frac{4}{\left[\left(\frac{\lambda_n}{\lambda_m}\right)^2 + (-1)^{m+n}\right]} \quad , \quad (1.46)$$

and

$$c_{nm} = \begin{cases} 4(\lambda_m \zeta_m - \lambda_n \zeta_n)/[(-1)^{m+n} - (\lambda_n/\lambda_m)^2] & ; m = n \\ \lambda_m \zeta_m (2 - \lambda_m \zeta_m) & ; m \neq n \end{cases} \quad . \quad (1.47)$$

The values  $\lambda$  and  $\zeta$  can be retrieved by curve fitting the data given by the book stating the relationship between mode number,  $L\lambda_m$ , and  $\zeta_m$ , Table 3.

Table 3. Dimensionless Analysis Data for Flow-Induced Vibrations (Blevins, 1997)

Mode #	$L\lambda_m$	$\zeta_m$
1	1.875	0.734099
2	4.694	1.018466
3	7.855	0.9992245

### 1.3. Thermofluids physics

The cold flow from the vortex tube will be used to dissipate 5 Watts of heat power that the laser is generating. The chamber contains a nozzle that will orient the air stream and form a thin film of cooling flow over the heated plate. During the cooling process, the resulting maximum temperature differential based on temperature distributions throughout the plate should be less than 100 mK. This is a forced convection process where the mechanics and heat transfer of the flow's interaction with the plate will be investigated.

#### 1.3.1. Fluid mechanics of flow over flat plate

The major outcomes of analyzing the mechanics of the flow consist of air velocities and shear stresses. In order to completely understand the development of the fluid flow throughout the length of the plate, the boundary layer thickness must be determined as a function of flow velocity and plate length. The boundary layer thickness for the general situation of a flow over a flat plate (Bergman et. al, 2011) is

$$\delta(x) = 0.38xRe^{-1/5} \quad , \quad (1.48)$$

for turbulent flows. ASML stressed out that the nozzle used for the application will develop turbulent flows exclusively due to its geometry despite the flow characteristics.

With boundary layer thickness solutions, the shear stresses can be determined throughout the plate. The shear stress for thin film flows over a flat plate (Bergman et. al, 2011) is defined as

$$\tau_w(x) = \frac{1}{2} \rho C_F u_\infty^2 \quad , \quad (1.49)$$

where  $C_F$  is determined for turbulent flows as

$$C_F = \frac{0.2}{x} \delta \quad . \quad (1.50)$$

Since vibrations are proportional to shear stresses, these must be minimized. Eqs 1.16 to 6.18, however, contain 4 unknown parameters, and thus, are indeterminate without the definition for the velocity of the flow at some position on top of the plate. For turbulent flows, the velocity profile is not straightforward to determine, however, empirical equations can be used. A very common empirical equation (Bergman et. al, 2011) for turbulent flat plate boundary layer velocity profiles is

$$\frac{u(x)}{u^*} = \frac{1}{\kappa} \ln \left( \frac{y u^*}{\nu} \right) + B \quad , \quad (1.51)$$

called the “Log Law”, where  $\kappa$  and  $B$  are turbulence model parameters considered constants ranging from 0.40-0.41 and 5.0-5.5, respectively, and

$$u^* = \sqrt{\frac{\tau_w}{\rho}} \quad . \quad (1.52)$$

This will allow for a solution of the velocities as a function of  $x$ , length throughout the plate.

### 1.3.2. Forced convection over flat plate

Convection is the transfer of heat between a body and a moving fluid that is constantly entering and leaving the control volume. Forced convection, rather than free convection, is the process of convection when the moving fluid has been previously condition for the purpose of

increasing the quality of heat transfer. Since a vortex tube is being used to cool a heated plate, this situation will be considered forced convection by thin film flow. The major components of these analyses will consist of general and transient convective heat transfer for understanding of thermal time constants and temperature distributions throughout the surface. Temperature distributions will depend mostly on velocities of the fluid flow, since convective heat transfer coefficients are usually contingent on these.

By considering changes of temperatures as differential, the conservation of energy equation can be rewritten as (Cengel et. al, 2014)

$$q_s'' A_{s,h} + \dot{E}_g - [h(T - T_\infty) + \varepsilon\sigma(T^4 - T_{sur}^4)] A_{s(c,r)} = \rho V c \frac{dT}{dt} \quad , \quad (1.53)$$

where constant surface heat flux, internal heat generation, radiation, and convective heat transfer are present,

Fig. 3. Eq. 1.20 is a “nonlinear, first-order, nonhomogeneous, ordinary differential equation that cannot be integrated to obtain an exact solution” (Cengel et. al, 2014).

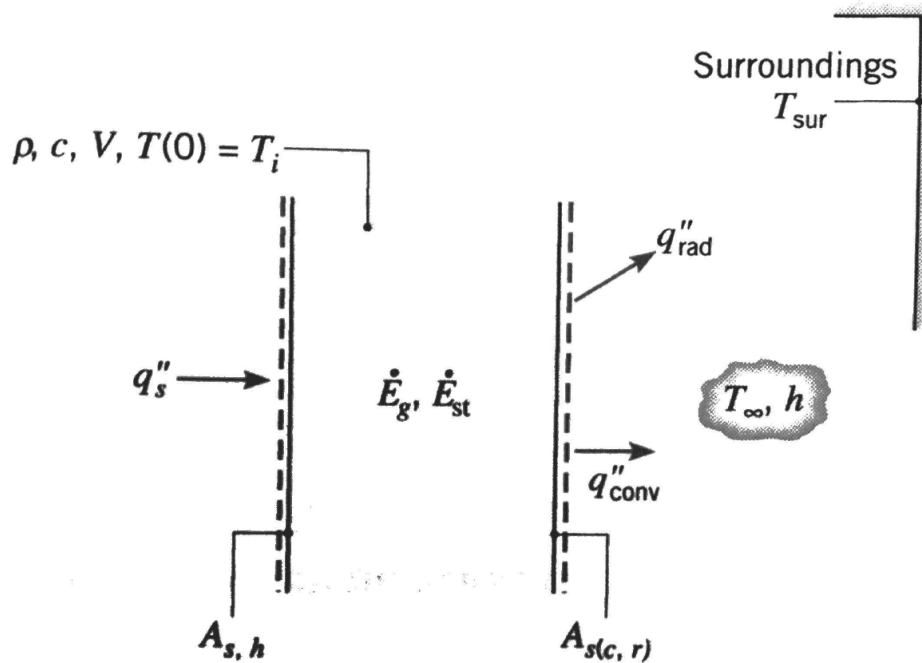


Fig. 3. Control surface for lumped capacitance analysis (Cengel et. al, 2014)

#### **1.4. Clean room requirements**

To keep the photolithography system as functional as possible, there are certain standards that must be maintained for the room it is in. These are considered clean room requirements.

There are several classifications for clean room requirements depending on what you are doing.

In this case, a simple standard must be abided. The room must be at STP or standard temperature and pressure. The room along with the chamber in the photolithography machine are both at STP. The environment to which the fluid flow will be entering will consist of atmospheric and ambient conditions.

## 2. General methodologies

A methodical flow chart to study the feasibility of the vortex tube was created to lay out the phases of the Design Analysis and Experimentation process, Fig. 4.

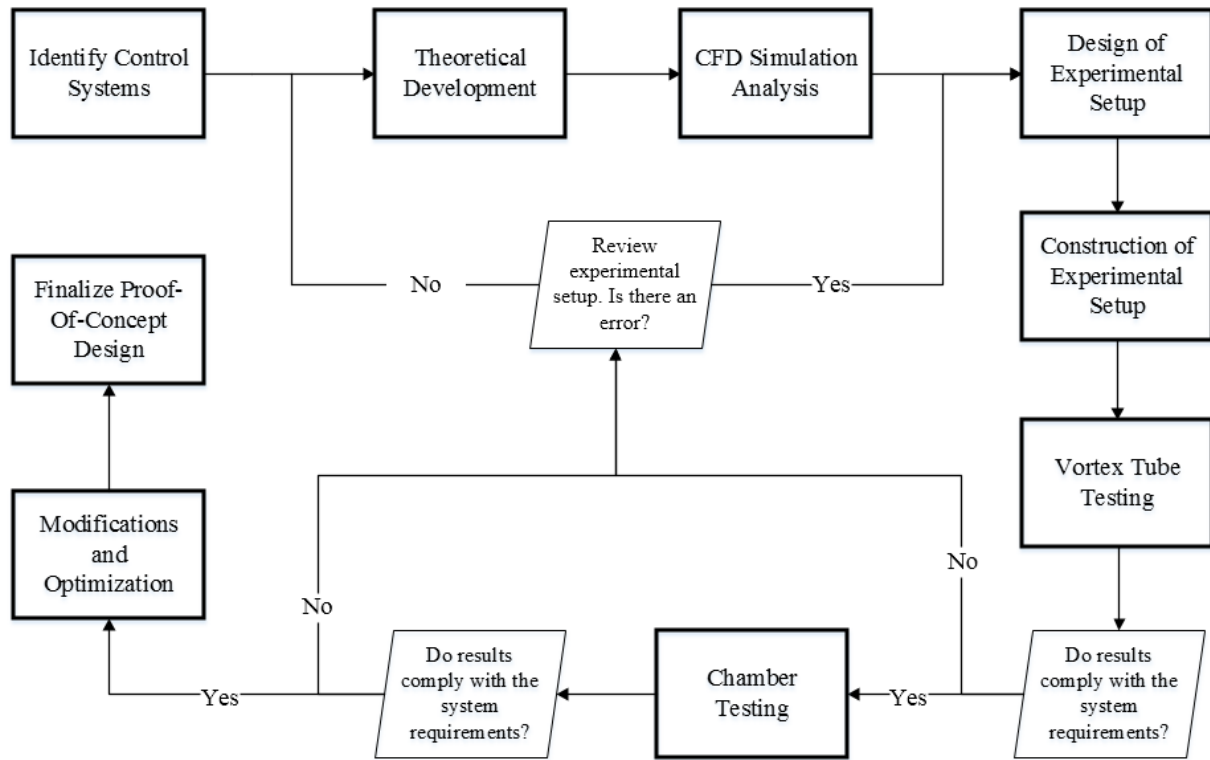


Fig. 4. Design process flowchart

The design process is organized by dividing the project in two main control systems, one of which consists of the chamber, Fig. 5, which may be referred to as the Chamber Control System (Chamber CS), and the second is vortex tube, which may be referred to as the Vortex Control System (Vortex CS).

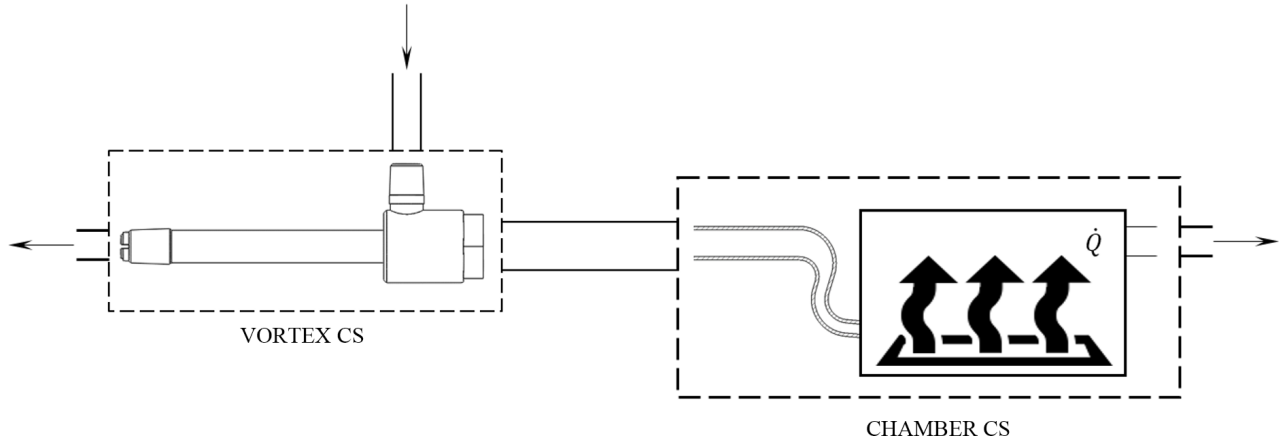


Fig. 5. Established control systems for facilitation of analyses

By dividing the system into two control systems, the theoretical development and the methods organization for the project are facilitated. Methods will consist of:

- Understand vortex tube capabilities and the vital flow characteristics from parametric analyses
- Perform thermofluids analysis on a flow over a flat plate
- Design the experimental setup, as well as experimental methods
- Model CFD simulations for the mechanics of a flow over a flat plate
- Conduct the designed experiments
- Using theoretical and experimental results to describe the demonstration and feasibility of the vortex tube for the application

### **3. Project schedule and tasks**

A project schedule, Appendix A, was established to aid the team with focusing on tasks that are time-sensitive and to ensure that all tasks will be completed on time and accurately. This project schedule lists all major activities through each academic term that the team is developing the project, and also assigns a student on the team to lead each task.

## 4. Theoretical development methods

### 4.1. Parametric analysis on vortex tube

Since Chamber CS analysis results are needed before fully developing a theoretical model of the Vortex CS, a parametric analysis is the best method to set about this. This way, the input parameters would be calculated as functions of the output, and will be able to be properly meshed with Chamber CS analysis results. To correctly analyze the thermodynamic and fluid-mechanics-related events that occur within this system, the performance charts that are provided for the specific vortex tubes must be used to completely characterize the vortex tube's capabilities regarding the cold fractions. Thus, each cold fraction listed in the said charts were curved fitted with respect to the input pressures. Within the working temperature ranges, the trend line that fit most perfectly was the log function, Table 3. Keep in mind, though, these functions are only used properly within pressure ranges of 0-6.9 bar (0-100 psi).

Table 4. Curve fitted log functions for medium vortex tube cold fractions

<b>Cold Fraction, <math>\epsilon</math></b>	<b>Log Function <math>\epsilon(p_0)</math></b>
0.2	$21.479 \cdot \ln(p_0) - 220.5$
0.3	$20.334 \cdot \ln(p_0) - 208.05$
0.4	$18.88 \cdot \ln(p_0) - 192.81$
0.5	$16.845 \cdot \ln(p_0) - 171.36$
0.6	$14.714 \cdot \ln(p_0) - 150$
0.7	$12.081 \cdot \ln(p_0) - 123.11$
0.8	$8.9516 \cdot \ln(p_0) - 90.727$

With these log functions, along with a step function, the temperature differential in the vortex tube could be identified as a function of both the cold fraction and input pressures, and thus, the temperature in the cold outlet is determined by

$$T_C(\varepsilon, p_0) = T_0 - T_{\Delta}(\varepsilon, p_0) \quad , \quad (4.1)$$

where  $T_{\Delta}(\varepsilon, p_0)$  consists of the step and log functions. The derivation of this equation can be found in Appendix B.1. A plot of Eq. 4.1 with respect to varying cold fractions and input pressures, Fig. 6, shows that high input pressures are necessary for the vortex tube to be able to operate at maximum cooling capacities.

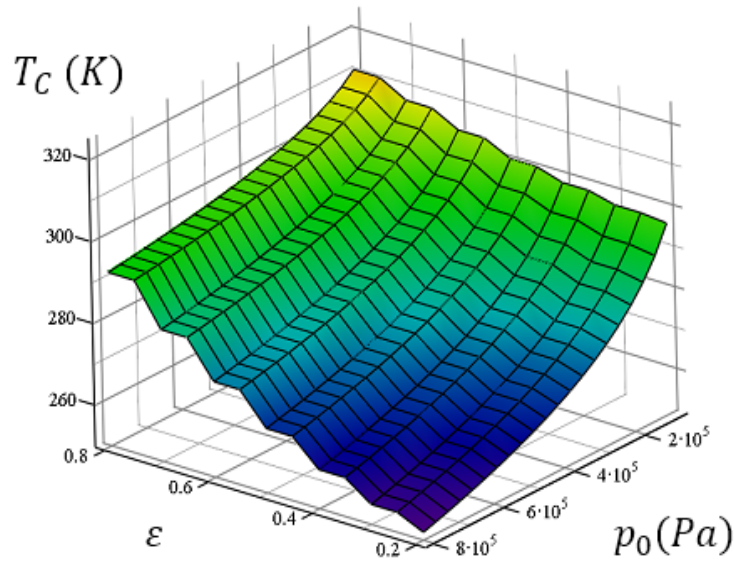


Fig. 6. Temperatures at cold outlet with varying cold fractions and input pressures

Additionally, for a lower cold fraction a lower temperature is achievable, and this is due to the law of conservation of mass/energy. Therefore, the higher the consumption of air that is allowed to leave through the hot outlet of the vortex tube, the lower the temperature difference

will be at that stream compared to the input stream. Similarly, for a higher cold fraction the higher the temperature difference will be at the hot outlet.

Thermal time constant theories have not been developed to present date for the vortex tube. The scope of this project did not allow for spare time for establishing studies on this. Therefore, thermal time constants will only be investigated experimentally.

The system must now be analyzed regarding the mechanics of the flow and the type of flow the vortex tube is producing depending on various input parameters. The best way of describing a type of flow is by determining the Reynold's Number of it. However, the Reynold's Number must be determined as a function of the controlled input parameters, which are:  $\dot{m}_0$ ,  $T_0$ , and  $P_0$ . With the normal definition of the Reynold's Number, implementations from the mass flow rate definition, the cold fraction definition, the Ideal Gas Law for density definition, and Polytropic conditions can be done for the full developed definition of the Reynold's Number in terms of the input parameters, for which the result is

$$Re_c(\varepsilon, p_0, \dot{m}_0) = \frac{4R\varepsilon\dot{m}_0T_c(\varepsilon, p_0)^{\frac{1}{1-\gamma}}}{\pi v d_c p_0 T_0^{\frac{\gamma}{1-\gamma}}}, \quad (4.2)$$

The plot in Fig. 7 shows that there is a correlation between the cold fraction and the input mass flow rate to the Reynold's Number of the flow of the cold stream. For a higher cold fraction, a larger Reynold's number is achievable, and this makes sense because in general, a larger consumption of flow rate will generate a higher Reynold's Number. Similarly, a higher Reynold's Number is produced for increasing input mass flow rates, which in turn, generate higher mass flow rates at the cold outlet for a specific cold fraction. The plot also shows that the pressure is indirectly proportional to the Reynold's Number of the cold stream flow. Therefore,

for a higher pressure, a lower mass flow rate and cold fraction, a higher degree of laminar flow is achievable.

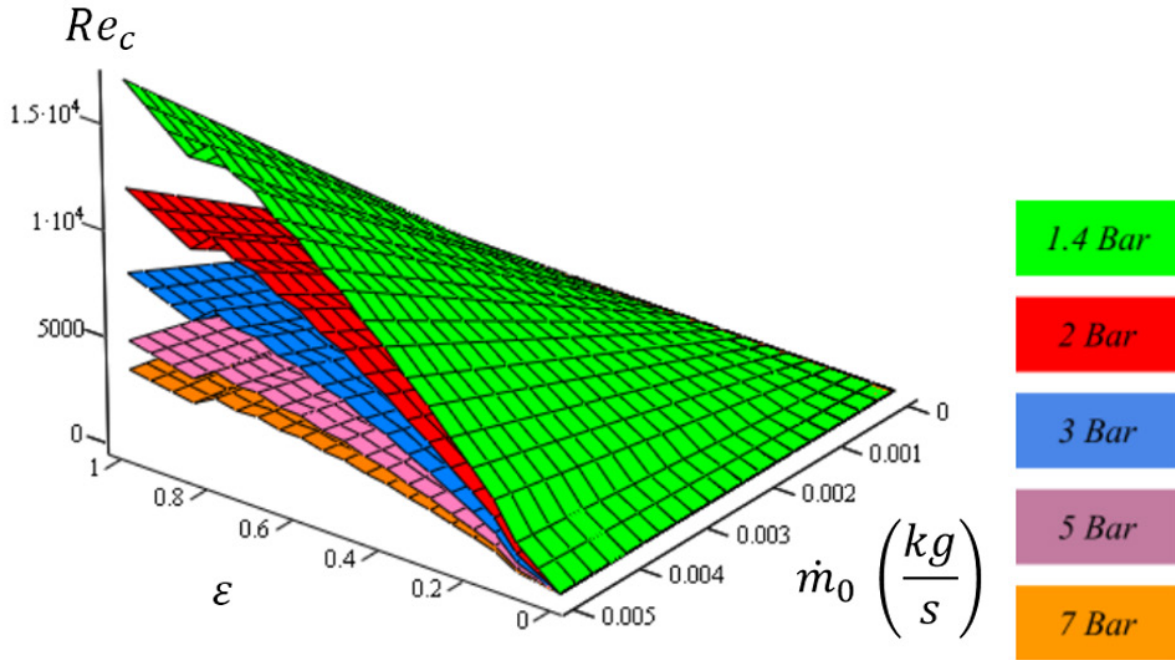


Fig. 7. Reynold's number for various input pressures, input mass flow rates and cold fractions

#### 4.2. Thermofluids analysis of vortex tube flow over flat plate

A thorough thermofluids analysis was performed to determine how to generate the flow needed to dissipate the heat power that is generated by the laser, specified by ASML. From the given information, the process will be reverse engineered to solve for parameters describing the flow exhausting from the nozzle. With this, the Chamber CS will be analyzed directly by plugging in varied input values and subsequently observing the effect these variations have on the behavior of the output parameters. The system situation will be treated as a 2-dimensional forced convection process of a fluid flowing over a horizontal flat plate.

The major outputs for the system consists heat dissipation, minimal plate vibrations and uniform temperature distributions over the plate. The components of the chamber include the flat plate and the nozzle, which will be orienting the cooled air into a thin film flow over the plate. The flow distribution and development throughout the plate for a general situation is comprised of increasing unsteadiness in the flow, which in turn will eventually force a transition to turbulence, Fig. 8. However, for this project, ASML stressed out that the nozzle will generate turbulent flow from the start due to its geometric shape, thus, the theoretical model will be developed solely for turbulent flows.

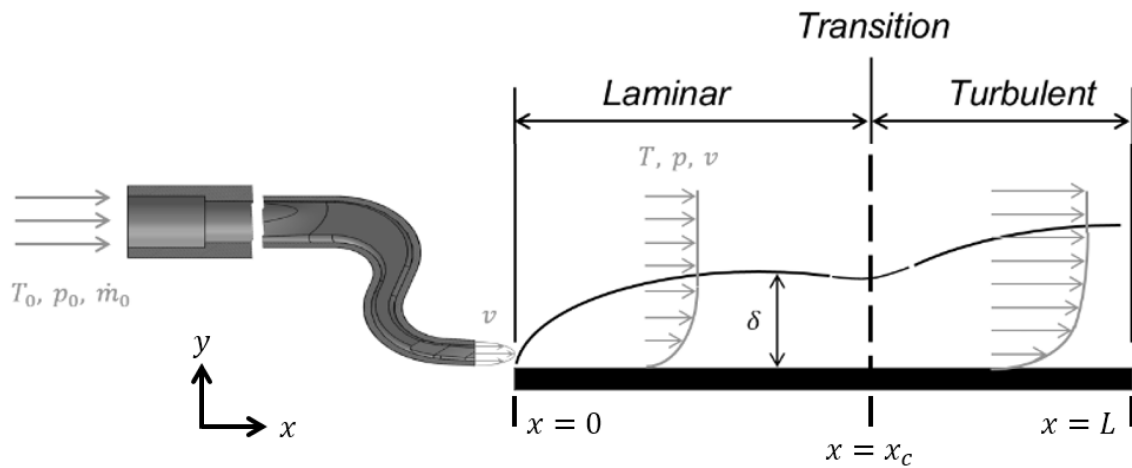


Fig. 8. Schematic representation of fluid exhaustion flow from the nozzle over the flat plate

#### 4.2.1. Velocity and boundary layer thickness profiles

Theoretical velocity distributions throughout the length of the plate will allow for a more complete definition of the boundary layer thickness profile. The log law empirical formula, Eq. 1.51, along with Eqs 1.48-1.50 and 1.52 can be used to solve for the velocity as a function of the distance along the length of the plate,  $U_\infty = u(x)$ , Appendix B.2. The result is

$$u(x) = \frac{0.316 v^{\frac{1}{10}} u_{\infty}^{\frac{4}{10}}}{\kappa x^{\frac{1}{10}}} \ln \left( \frac{0.316 y u_{\infty}^{\frac{4}{10}}}{v^{\frac{1}{10}} x^{\frac{1}{10}}} \right) + \frac{0.316 B v^{\frac{1}{10}} u_{\infty}^{\frac{4}{10}}}{x^{\frac{1}{10}}} . \quad (4.3)$$

Since  $\delta$  was used to substitute the  $y$  term in Eq. 1.51, Eq. 4.3 is the solution for the velocity distribution throughout the distance along the length of the plate when the velocity as a function of the distance perpendicular to the plate is maximum. In other words, Eq. 4.3 is a solution for the velocity in the  $x$ -direction above the boundary layer thickness. Herewith, the boundary layer thickness profile and shear stress distributions are directly calculated. The boundary layer thickness throughout the length of the plate for an inlet velocity of 9 m/s is determined by

$$\delta(x) = \frac{0.37x^{4/5}v^{1/5}}{\left[ \frac{0.316 v^{\frac{1}{10}} u_{\infty}^{\frac{4}{10}}}{\kappa x^{\frac{1}{10}}} \ln \left( \frac{0.316 y u_{\infty}^{\frac{4}{10}}}{v^{\frac{1}{10}} x^{\frac{1}{10}}} \right) + \frac{0.316 B v^{\frac{1}{10}} u_{\infty}^{\frac{4}{10}}}{x^{\frac{1}{10}}} \right]^{1/5}} . \quad (4.4)$$

Now, the boundary layer has been completely identified. Before verifying the shear stress that the flow creates regarding the boundary layer, it is helpful to visualize how influential is the inlet mass flow rate on the boundary layers. See Fig. 9 for a 3D representation graph of the boundary layer for varying length distances and exhaust mass flow rate.

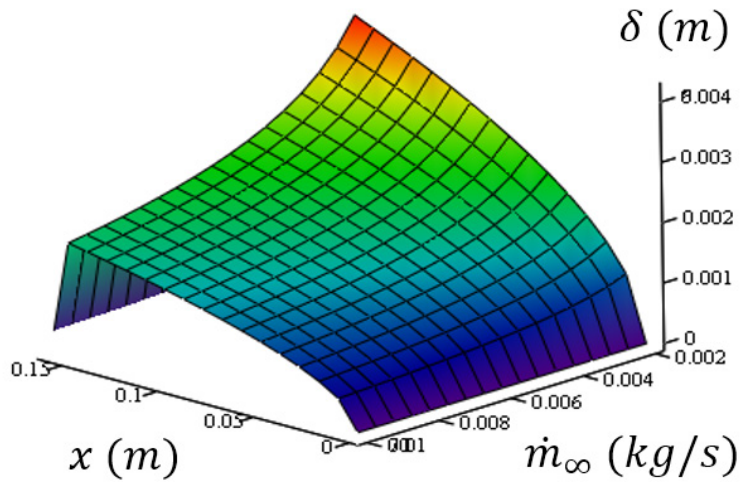


Fig. 9. Boundary layer plotted over plate length for various flows

Now, the shear stress needs to be defined as a function of the boundary layer thickness. Here, the critical parameter that will come into play is the Skin Friction Coefficient,  $C_F$ , which directly relates the boundary layer thickness to the respective shear stress it creates. To recall, the shear stress can be determined in terms of the skin friction coefficient, which will be a function of the boundary layer thickness.

#### 4.2.2. Lumped capacitance for transient heat dissipation

Fig. 10 shows a schematic diagram of the plate with all of the different types of heat transfers that are present in the system.

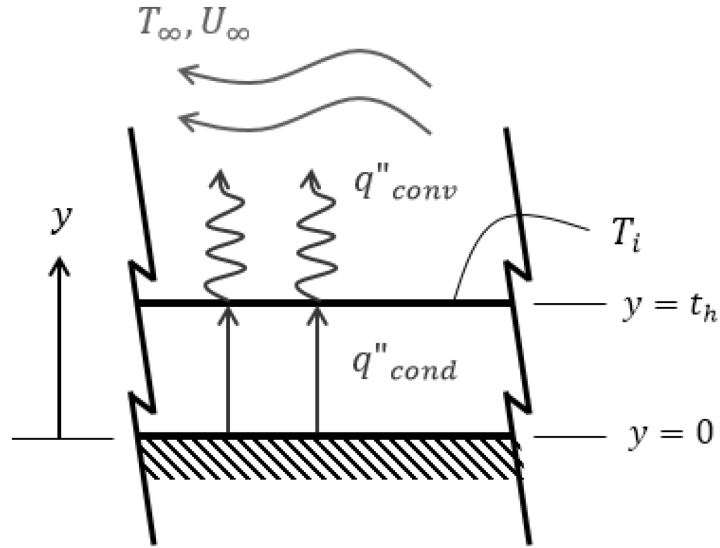


Fig. 10. Schematic representation of heat transfers in the plate

To calculate the transient heat dissipation rate, the surface of the plate was considered a control volume. Beforehand, the Biot number must be determined and verified for validation with the Lumped Capacitance method, which is

$$Bi = h_c \frac{L_c}{k} \quad . \quad (4.5)$$

If the convective heat transfer coefficient,  $h_c$ , is assumed to be roughly  $25 \text{ W}/(\text{m}^2\text{K})$ , the Biot number comes up to be  $1.014E - 3$ , which is well within the ranges for validating the lumped capacitance method for a certain application. Therefore, the conservation of energy equation with application of transient conditions, Eq. 1.21, is validated for this application. The equation was simplified by neglecting radiation and internal heat generation, for which the end result is

$$q''_s A_{s,h} - h A_{s(c,r)} (T - T_\infty) = \rho V c T' \quad , \quad (4.6)$$

which is an ordinary first order linear differential equation. The solution is

$$T(t) = \frac{q_0}{h_c} \left(1 - e^{-\frac{t}{\tau}}\right) + T_\infty \left(1 - e^{-\frac{t}{\tau}}\right) + T_0 e^{-\frac{t}{\tau}} \quad (4.7)$$

With the aid of Eq. 4.7, the temperature profile throughout time at the surface of the plate was identified. A 3D plot representation of the convective heat cooling process for the surface temperature shows the temperature profile throughout time for various air flow temperatures.

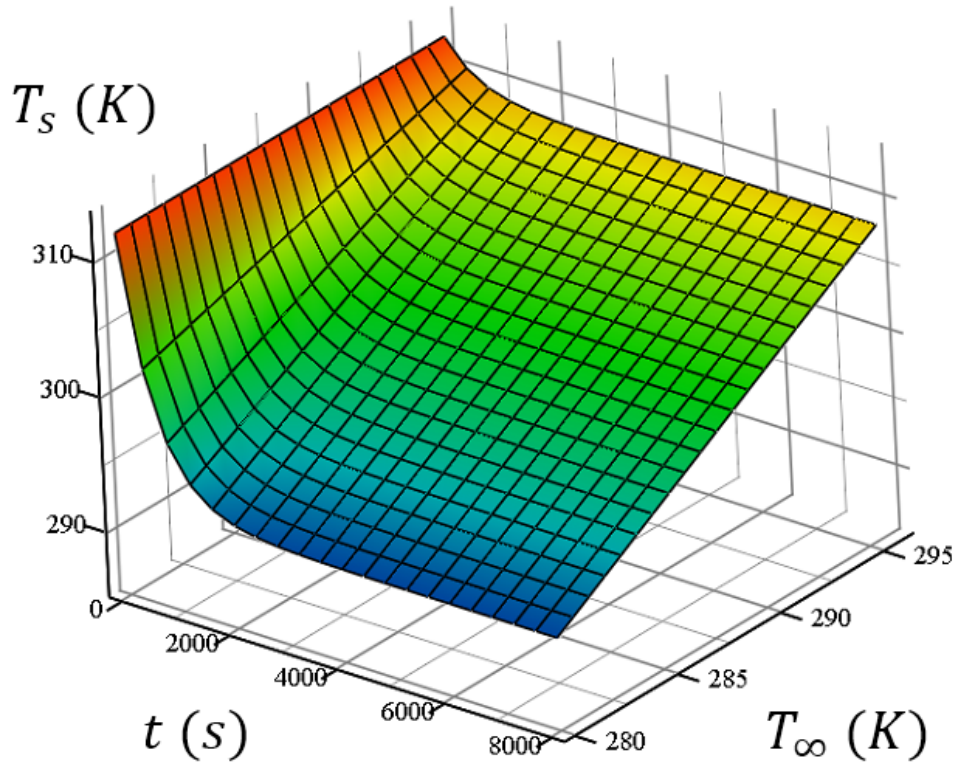


Fig. 11. Surface temperature of the plate for various cooling flow temperatures over time

To dissipate the 5 Watts of heat power being added to the plate, a horizontal slice on the plot from Fig. 11 is made at the desired final temperature. By doing this, the temperature of the flow that needs to be exhausted over the plate is determined to be roughly 14 °C, assuming the convective heat transfer coefficient between the flow and the plate is approximately 25 W/(m<sup>2</sup>K).

## 5. Computational simulation methods

Simulations for the mechanics of the thin film flow being exhausted over a flat plate were completed using the Computational Fluids Dynamics (CFD) software tool COMSOL to further improve and validate calculations and design. A SolidWorks CAD replica of the chamber cavity, along with the outlet of the nozzle provided by ASML, was set up to be the geometric model representation in the CFD software. Since the nozzle generates unsteadiness in the flow, which in turn produce turbulence, due to its geometry, the flow was simulated as turbulent. Turbulence modelling was done using the  $k-\epsilon$  method, which is the most common turbulence modelling strategy used in similar applications. Fig. 12 shows the complete final tree manager, or “Model Builder”, for COMSOL. Detailed steps for modelling the simulation, after completing the geometry and importing it to the software, are listed in Appendix C.

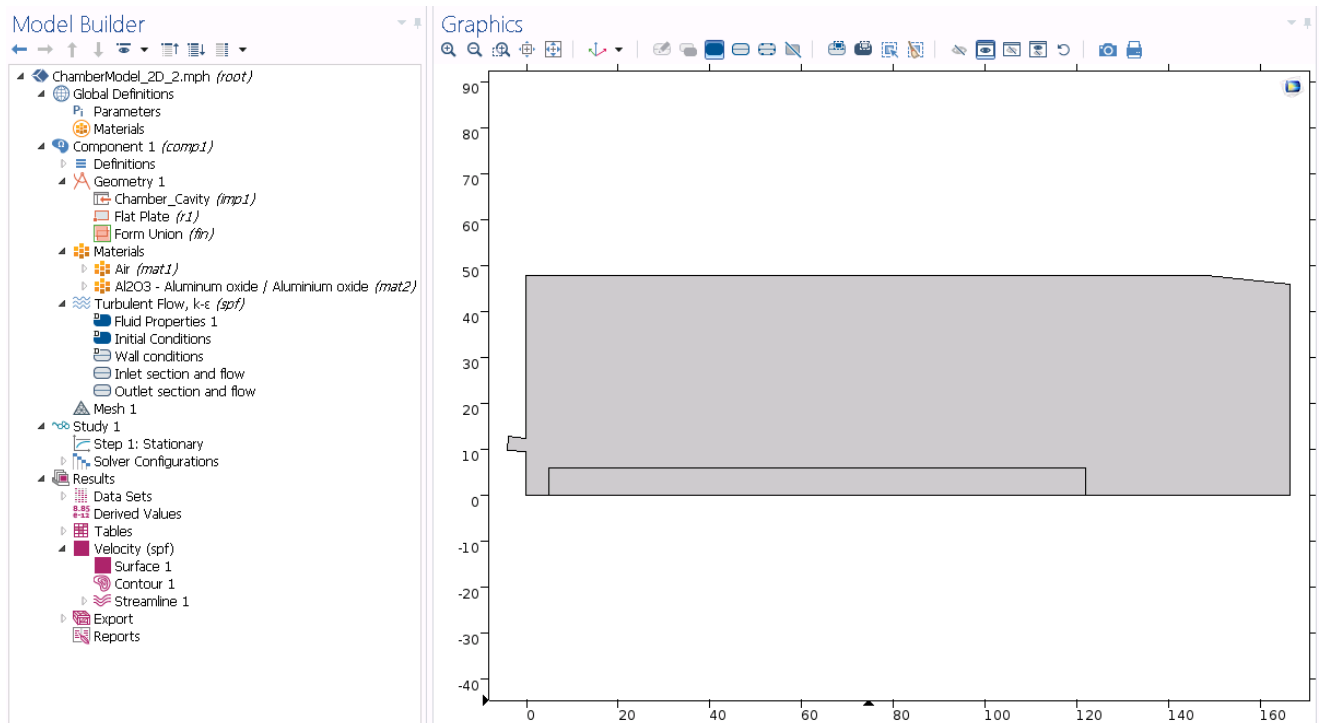


Fig. 12. Expanded tree manager and geometry after modelling the simulation in COMSOL

## **6. Experimental methods of a vortex tube's capabilities and limits**

### **6.1. Design of experiments**

The experiments for the vortex tube should test its capabilities and characterize it regarding the main flow parameters and thermal time constants. The focus of these experiments are collecting temperature-dependent data of output parameters when the input are strategically varied. To recall, the main parameters are the following: cold fraction, input pressure, and input flow rate. However, since a specific amount of flow rate must be provided to the chamber in order to maximize the convective heat transfer coefficient, the cold temperature data from variations of the input flow rate will not be investigated. The experiments designed for testing the vortex tube's performance investigate optimal input parameter values, and are organized in Table 5. These consist of monitoring the cold temperatures of the flow at the cold outlet over time when the main parameters, cold fraction and input pressure, are varied in specific ranges. All of the collected data points contain a response time, which means they can be plotted over time to investigate the thermal time constants from a specific parameter value to the next, after achieving steady state.

Table 5. Designed experiments for vortex tube performance testing

Main parameters	Designed experiments
<ul style="list-style-type: none"> <li>• Input Temperature</li> <li>• Input Pressure</li> <li>• Input Flow Rate</li> <li>• Cold Fraction</li> <li>• Cold Temperature</li> <li>• Hot Temperature</li> </ul>	<ul style="list-style-type: none"> <li>• Create a vortex tube performance chart                             <ul style="list-style-type: none"> <li>• Collect temperature data for varying cold fractions</li> </ul> </li> <li>• Determine optimal pressure for maximum cooling capacity                             <ul style="list-style-type: none"> <li>• Collect temperature data for varying input pressures</li> </ul> </li> <li>• Find the thermal time constants for temperature dropping                             <ul style="list-style-type: none"> <li>• <math>\Delta T_{Cold}(\epsilon, t)</math></li> <li>• <math>\Delta T_{Cold}(p, t)</math></li> <li>• Define a method of reducing the thermal time constants                                     <ul style="list-style-type: none"> <li>• “Forced Experiment” - Set temperature from ambient to a desired temperature with manipulation of the parameter with the lowest thermal time constant</li> </ul> </li> </ul> </li> </ul>

## 6.2. Design of experimental setup

The main sections of the experimental setup consist of conditioning and measuring, where the air stream will be conditioned and measured in terms of flow rate and pressure. The temperature will not be conditioned, because the vortex tube works in relative scale from the input temperature. In other words, the vortex tube will provide readings of temperature differences from input to output, thus there is no need for temperature conditioning. Fig. 13 shows a block diagram containing the main sections of the experimental setup; within these, specific equipment will be chosen.

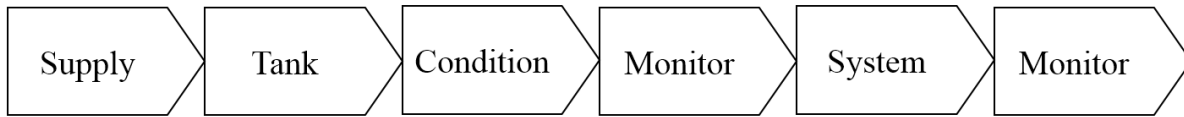


Fig. 13. Vortex tube experimental setup block diagram

From the supply, the air must be contained within a tank/accumulator to be able to efficiently control the air that is fed into the vortex tube. Pressure regulators were placed at the inlet and outlet of the accumulator. Afterwards, as part of the conditioning section, a pneumatic flow control valve will be used to control the flow rate of the input stream. The stream will then be measured prior to entering the vortex tube with the use of a sensor component that will be monitoring the velocity and temperature of the flow. This same component will also be placed on both output streams, as a means to correctly investigate the efficiency of the vortex tube in dividing the flows regarding temperature separation. The pressure will also be measured following the velocity/temperature sensors at each output stream, and then the streams will be exhausted into the ambient room. Additionally, the sound levels will be monitored at all times with the use of a sound meter. Fig. 14 shows a schematic representation of the experimental setup.

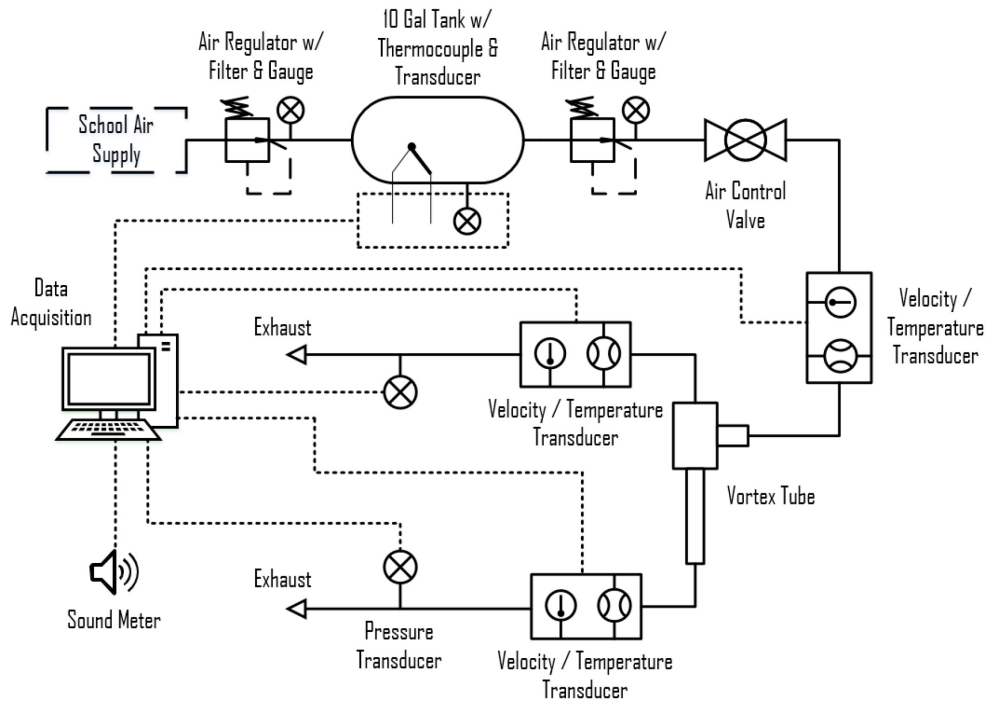


Fig. 14. Schematic diagram of the developed experimental setup for vortex tube testing

In addition to the schematic diagram, a 3D Computer Aided Design (CAD) model was created in SolidWorks, Fig. 15. This model would allow for verification against arbitrary and miscellaneous details that could potentially issue setup errors. The manufacturers for the specific components, Omega, McMaster-Carr, among others, provided in their websites either CAD models or detailed engineering drawings/dimensions of each piece of equipment.

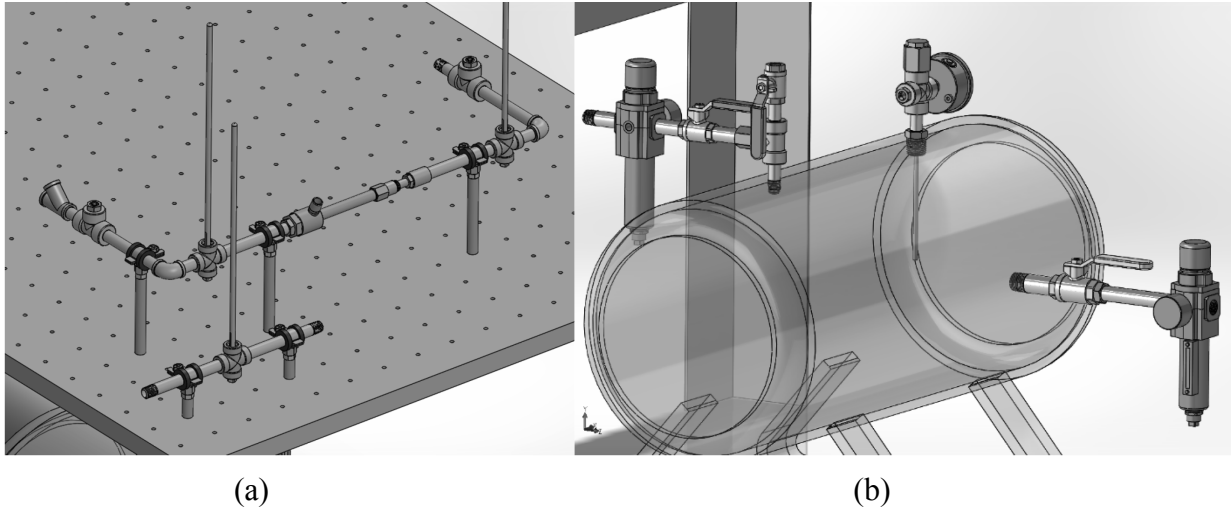


Fig. 15. SolidWorks CAD model of the setup (a) at the vortex tube, and (b) at the accumulator

### 6.3. Experimental procedures

For the first designed experiment, the varying parameter is the cold fraction. Meanwhile, the inlet mass flow rate is  $0.0059 \text{ m}^3/\text{s}$  (12.5 cfm), and the input pressure is 5.5 bar (80 psi). The experiment begins by filling the accumulator with pressurized air from the supply wall. The air is then regulated out of the tank in terms of pressure to 5.8 bar (85 psi), because there is a pressure drop throughout the flow control valve of 0.35 bar (5 psi). This pressure drop depends on the total pressure. The air is then supplied to the vortex tube while the cold fraction is at 100%. The cold fraction is then varied to 87.5%, 75%, 62.5%, and 50%, after achieving steady state at the cold outlet flow for each change in cold fraction. The experiments will not be performed for a cold fraction of less than 50%, because cost-effectiveness is a critical factor for the feasibility of the vortex tube. A cold fraction of less than 50% would mean that more than half of the compressed air being fed into the vortex tube is wasted. Therefore, the cost efficiency for this situation would be too low. Meanwhile, sound levels are being measured with a sound meter.

The varying parameter for the second experiment is the input pressure. The inlet mass flow rate and cold fraction throughout this experiment are the same as the previous and 87.5%, respectively. The same pre-processing from the previous experiment is done for this. The air is regulated out of the tank to 1.5 bar (21 psi) to account for the 0.1 bar (1 psi) pressure drop at the flow control valve. The air is fed into the vortex tube and steady state is achieved. The pressure is then regulated to 2.8 bar (40 psi), 4.1 bar (60 psi), 5.5 bar (80 psi), and 6.9 bar (100 psi), while accounting for the pressure drops of each pressure at the valve and reaching steady state during every change.

#### **6.4. Data acquisition logic process**

In order to collect accurate data from experiments, an experimental data acquisition system was developed based on the resources available to the team. The system that was developed consisted of a National Instruments DAQ-6229 data acquisition hub and a VI program made using LabVIEW 2015. This was based on the team's previous experience with both the NI hardware and the LabVIEW program, as well as the availability of both resources.

When developing the VI used for the experimental phase of the project, several considerations were made about how to collect the data and digitize it into usable results that would verify the theoretical analysis completed earlier in the project. One consideration was to find the best way to convert the analog output signals that the sensors used into accurate readings of the parameters the sensors were supposed to report. The sensors used for the experimental setup all output a certain range  $V_{dc}$ , this was dependent on the range of parameters the sensors were able to read. However, the  $V_{dc}$  output did not read what was desired, therefore, the VI was designed to be able to convert these output ranges into accurate parameters. Another

consideration that had to be made when creating the VI was that the program had to be able to accommodate different types of sensors used to read the system's output parameters.

In broad terms, the ideal VI that needed to be developed had several specifications that it needed to provide to accurately record the data desired from the experiments. These specifications consisted of:

- Providing accurate readings and displays for each individual sensor
- Accommodate any calibration or offsets from the sensors used
- Be able to document the results of every experiment performed in a clear and concise manner

## **7. Experimental methods of a vortex tube's integration in the designed chamber**

### **7.1. Design of experiments**

In order to investigate the amount of heat dissipation for a control cooling flow from the vortex tube, and the resulting temperature distributions, a simple heating and cooling experiment was designed. This experiment consists of replicating the 5 Watts of heat power on the plate until reaching steady state, and subsequently connecting the vortex tube's cooling flow to the nozzle for producing the thin film flow and forcing convective heat transfer until the plate is cooled to steady state. In the experiment, data points consisting of response times will be collected. This will allow for visualizing temperature distributions plots throughout time.

### **7.2. Design of experimental setup**

The setup for these experiments is an addition to the setup for the vortex tube experiments starting from the cold outlet of the vortex tube. The cold flow will be fed into the nozzle and subsequently exhausted onto the plate. The two main groups of instrumentation are monitoring and environment replicating. Heat power is replicated throughout the plate with the use of a plate heater. The main parameter that is monitored is the temperature at the surface of the plate, in terms of magnitude and distribution throughout the length of the plate. For data collection, thermocouples were placed strategically throughout the surface of the plate, as well as the use of an infrared camera for accurate readings on the distributions. Fig. 16 shows a schematic diagram of the complete experimental setup after the addition of the instrumentation for these experiments.

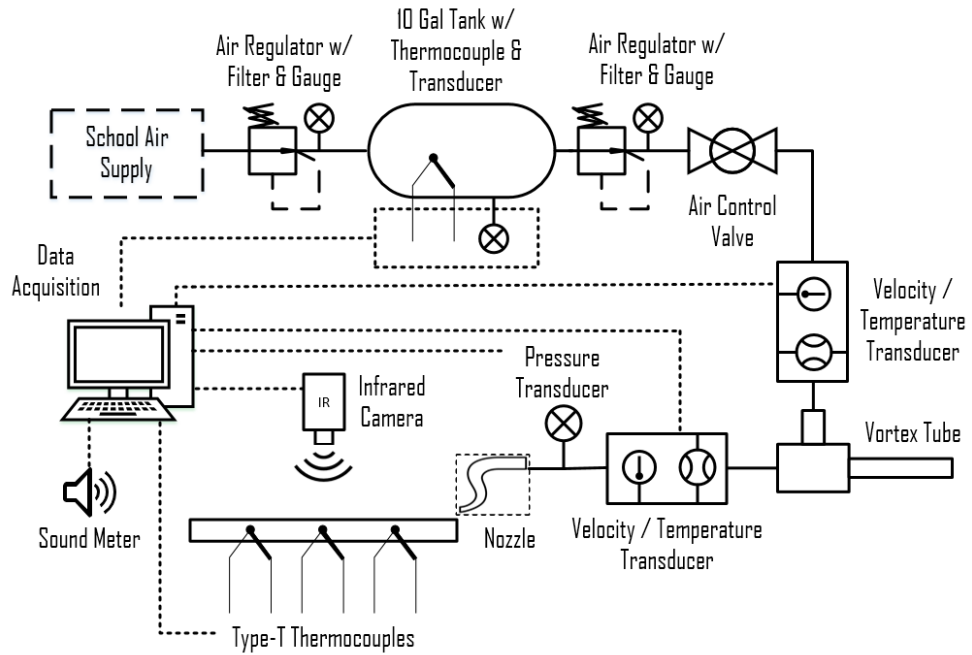


Fig. 16. Schematic diagram of the developed experimental setup for chamber testing

In addition to the schematic diagram, CAD of the chamber was designed in SolidWorks for facility of additive manufacturing, Fig. 17.

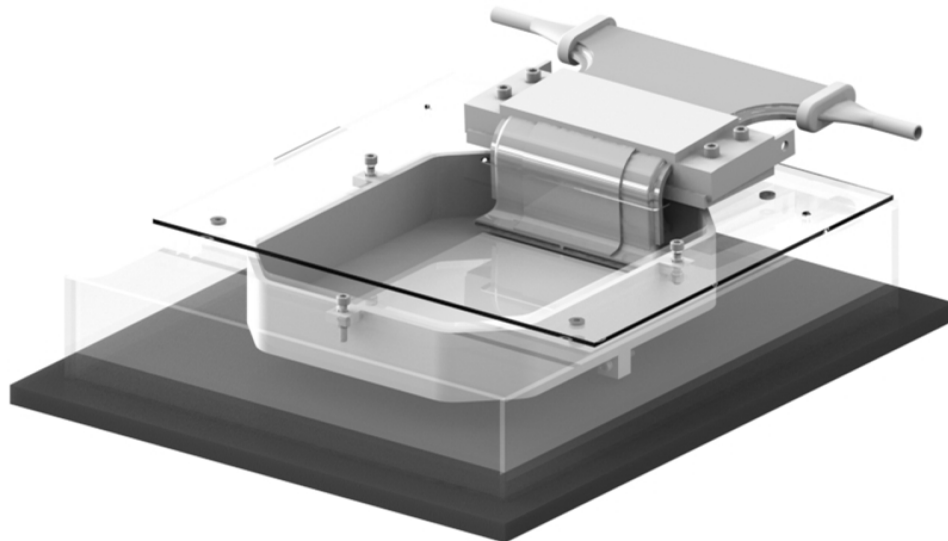


Fig. 17. Chamber CAD designed in SolidWorks

### **7.3. Experimental procedures**

Heating and cooling are the two main sections for these experimental procedures. First, the 5 Watts of heat power is replicated with the use of the plater heat until reaching steady state at the surface of the plate. In parallel, pressurized air is fed onto the vortex tube, while being disconnected from the nozzle. This is because the flow at the cold outlet must be at steady state before being fed into the nozzle. The cold fraction, input flow rate, and input pressure at the vortex tube were 90%, 0.0059 m<sup>3</sup>/s (12.5 cfm), and 5.5 bar (80 psi), respectively. These were chosen after analyzing the results of the vortex tube experiments. After achieving steady state at both the heated plate and the vortex tube's cold outlet flow, the vortex tube was connected to the nozzle in order to start the cooling process of the plate. Data is then collected until reaching steady state cooling at the plate.

## 8. Facilities and instrumentation

The facilities available for use were in Higgins Laboratories, an academic facility on WPI's campus. The lab used is supervised by the project advisor, Prof. Cosme Furlong-Vazquez. In order to attain high quality and accurate results, the instrumentation and apparatus used for this project were required to be high resolution and compatible with the facilities available for experimental use, Fig. 18. A detailed list of the instruments used for experimentation is found in Appendix D. The instrumentation consisted of several categories of items:

- Connection (piping, fittings)
- Conditioning (accumulator, pressure regulators, control valves)
- Monitoring (sensors)
- Environment replicating (additively manufactured chamber, plate heater, ceramic plate)

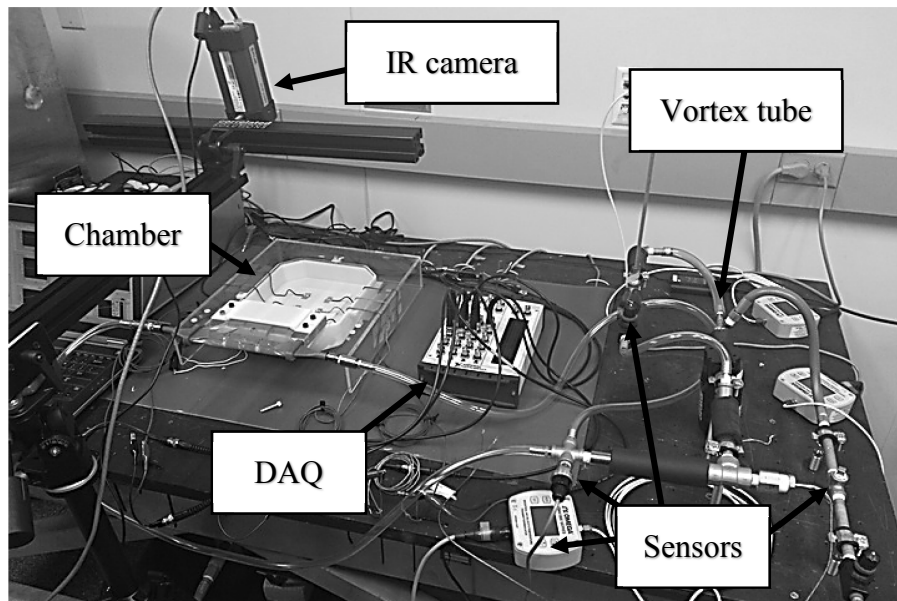


Fig. 18. Picture of assembled setup at the provided facility

### 8.1. Chamber construction

With the use of the instruments and apparatus used for these experiments, Section 8, the chamber was constructed. The chamber frame was made by cement-welding  $\frac{1}{4}$ " thick acrylic sheet pieces, which were laser cut to specified sizes, Fig. 19.

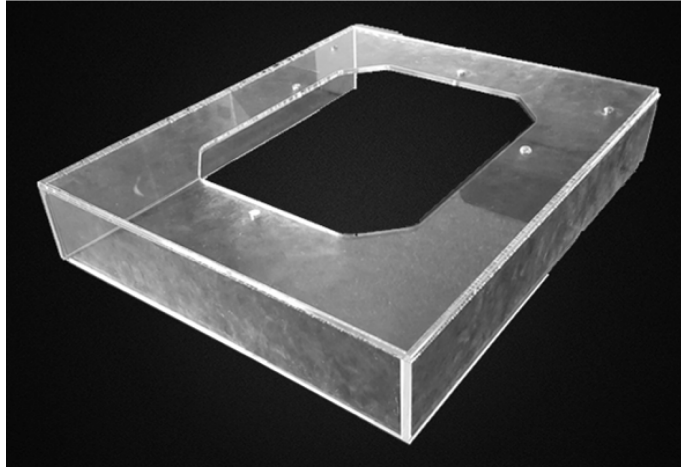


Fig. 19. Assembled chamber frame with welded acrylic sheets

An acrylic sheet was used and laser cut for serving as a cover for the chamber, which is needed based on ASML's given specifications. The chamber cavity, which is the area where the nozzle is exhausting the flow, was designed in SolidWorks and fabricated with rapid prototyping. The flexible plate heater was placed on a piece of wood in order to provide the necessary height, as well as insulation. This way, the heater could only generate heat upward, instead of both upward and downward. The heater produces the heat from an external power supply by receiving current through a wire that is patterned in a serpentine-like shape. Therefore, to heat the plate with evenly-distributed heat through the surface, a glass plate is placed between the heater and the alumina ceramic plate, Fig. 20. Assembling of the chamber with instrumentation. The thickness of the plate was chosen to be  $\frac{1}{4}$ ".

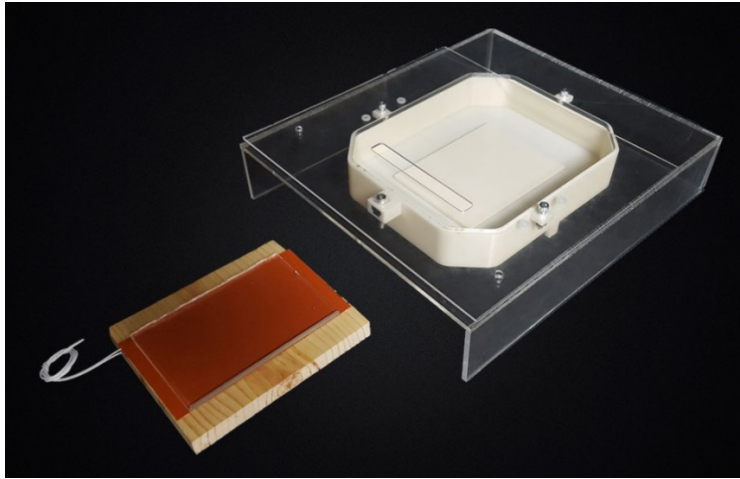


Fig. 20. Assembling of the chamber with instrumentation

Custom couplings were 3D printed for the nozzle, as well as a custom support to be able to hold the nozzle and easily mount it in additional supports designed specifically for providing angles. Afterwards, the nozzle, along with the heater and its respective mounting components, are incorporated in the chamber, Fig. 21.

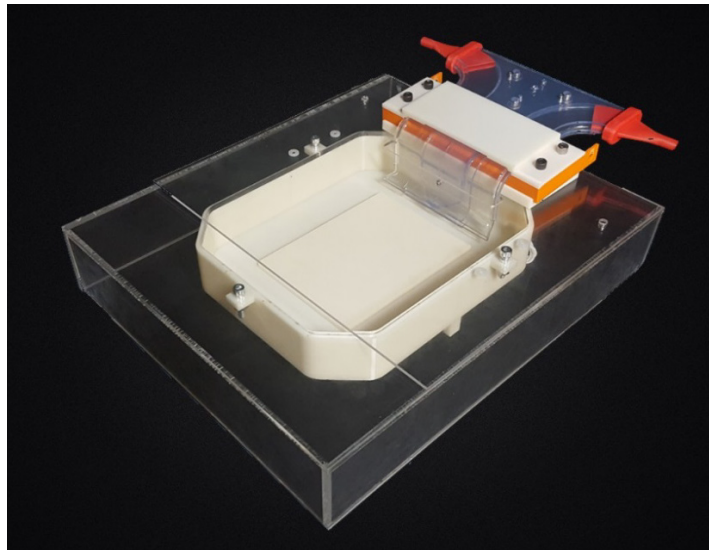


Fig. 21. Constructed chamber for experimentation

## 8.2. Monitoring Instrumentation

Due to the highly precise requirements ASML provided for the vortex tube to be considered viable, it was important that the sensors used for experimentation were high resolution and were able to detect a fine degree of variation in the system. Therefore, several sensors were selected based on this to provide the most accurate results for ASML.

The first sensor chosen was a dual-purpose air temperature and velocity sensor, Fig. 22. Three were used in the experimental setup. These sensors were made by Omega Engineering, and are the FMA1000 Series Temperature/Velocity Transmitters. The specific model of this sensor used was the 1003-R V1, which could measure from 0 to 10,000 FPM velocities, with an accuracy of  $\pm 1.5\%$  for velocity readings. The sensor has a readable temperature range was from -40 to 121 C, with an accuracy of  $\pm 0.5\%$  for temperature readings.



Fig. 22. Omega FMA1000-R V1 air velocity/temperature transmitter

To measure the pressure fluctuations in the system, another sensor was identified and purchased in multiple for the locations already specified in the designed experimental setup. The

pressure transducer purchased was the Omega PX-181B series, Fig. 23. The particular model purchased was the PX181B-100G5V, which has a measurement range of 0 to 100 psi. The pressure transducer provides readings with an accuracy of  $\pm 0.3\%$ .



Fig. 23. Omega PX-181B-100G5V pressure transducer

For thermal monitoring of the surface temperature distributions resulting from transient heat convection from the cooling flow, type-T thermocouples were used. The thermocouples purchased are McMaster-Carr surface thermocouples. The instruments are rated from 0 to 260 C, with a reading accuracy of  $\pm 0.75\%$ . Additionally, a high sensitivity FLIR SC6000 series infrared camera was used for recording thermal images of temperature distributions, consisting of an accuracy of  $\pm 2\%$  of reading.



Fig. 24. Infrared camera FLIR SC6000 series (FLIR)

## 9. Results and discussions

### 9.1. Computational and theoretical comparisons

Under a 2D plot group, a surface contour plot was generated for the velocity. The color scale and style, for visual purposes, is rainbow, Fig. 25. Velocity ranges throughout the length of the plate are approximately from 9 to 5 m/s.

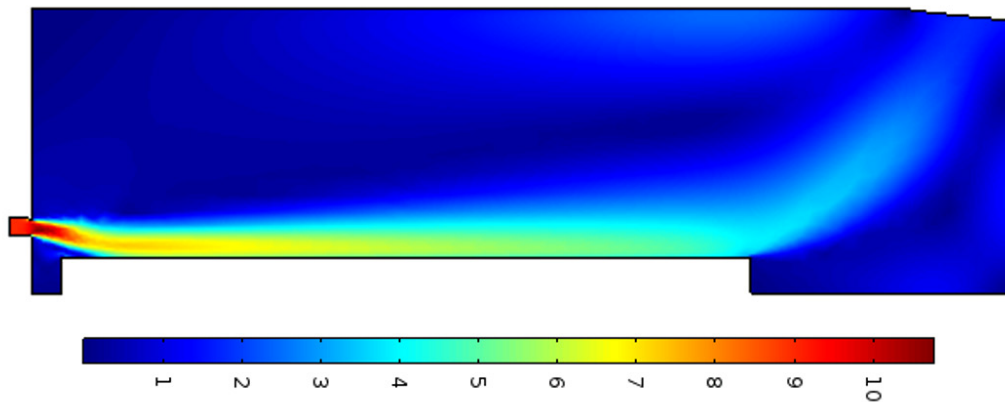


Fig. 25. Velocity (m/s) contour plot with rainbow color scale in COMSOL

A streamline was also plotted from the center of the inlet. Velocity magnitudes for each data point of the streamline throughout its trajectory were exported and plotted in a 1D plot graph, Fig. 26. Alongside, Eq. 4.3, Section 4.2.1, is plotted to show the comparisons between the two models. Considering that the theoretical model describes the velocity magnitude at the boundary layer, rather than through the path of a streamline, the comparisons are relatively good. The similarities discuss the validation of both models for declaring final conclusions on these analyses, regarding temperature distributions.

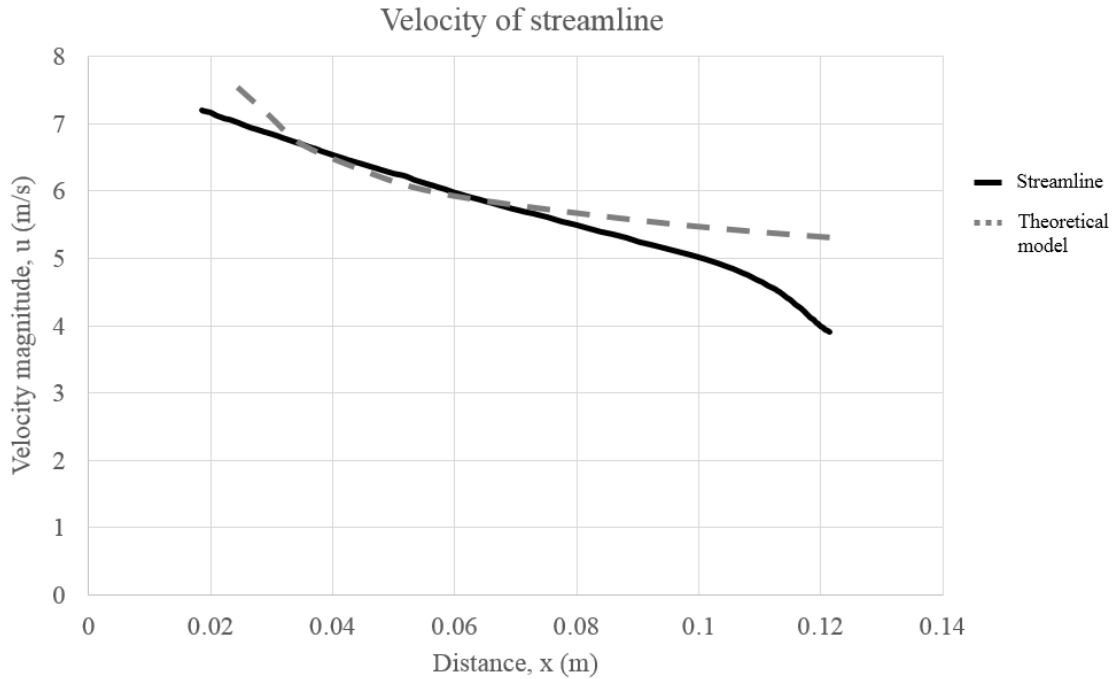


Fig. 26. Comparison of COMSOL streamline velocity data to theoretical model

## 9.2. Experimental results of a vortex tube's capabilities and limits

With the use of the specific instrumentation chosen for these experiments, the experimental setup was constructed following the schematic design discussed in Section 6.2. As mentioned, at the lab a table was provided and measured to ensure what section of the setup best fits on it. Due to the size of the accumulator, it was placed below the table. Thus, the setup consisting of every component from the wall outlet to the pressure regulator at the exit of the tank was placed under the table, Fig. 27. These consist of the following:

- Tubing from the wall outlet to the inlet of the tank
- Monitoring instrumentation at the tank: thermocouple, pressure gauge and transducer.
- Pressure regulators at the inlet and the outlet of the accumulator

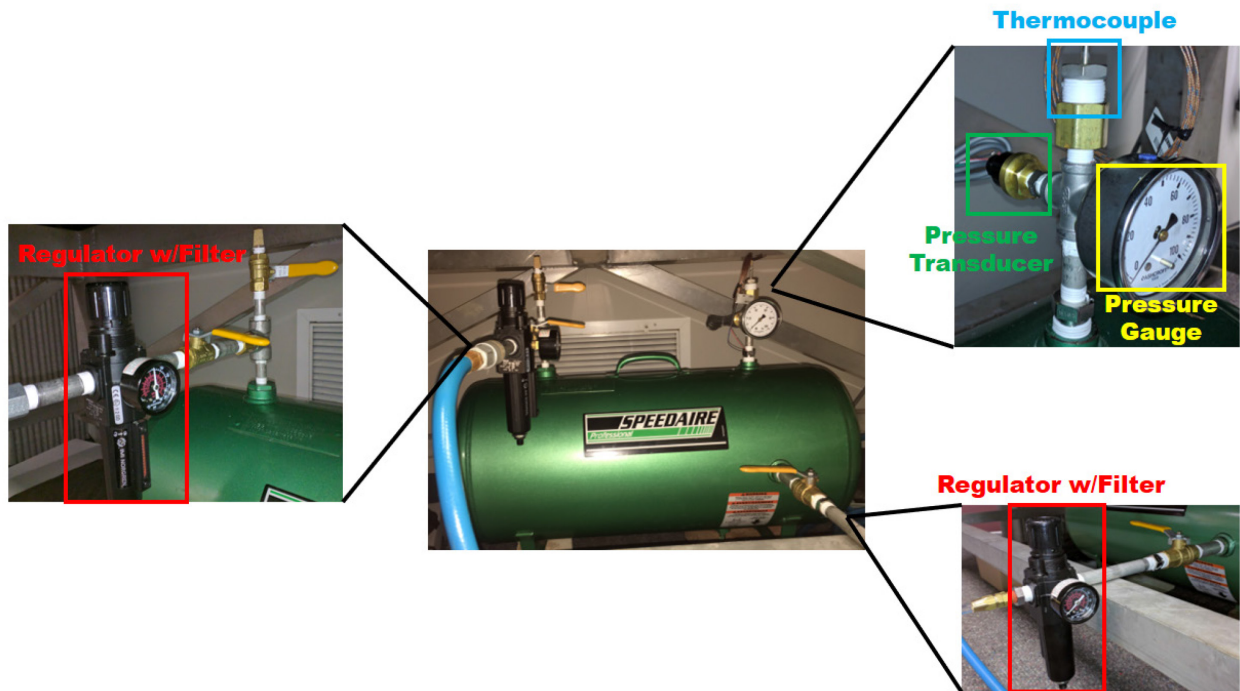


Fig. 27. Experimental setup showing accumulator, pressure regulators and monitoring sensors

The setup on top of the table, Fig. 28, consisted from conditioning the flow rate to the exhaust. More specifically, the following major components:

- Flow control valve
- Flow/temperature RTD sensors
- Pressure transducers
- Vortex tube: adjustable for small and medium sizes
- Exhaust outlets
- Data Acquisition box

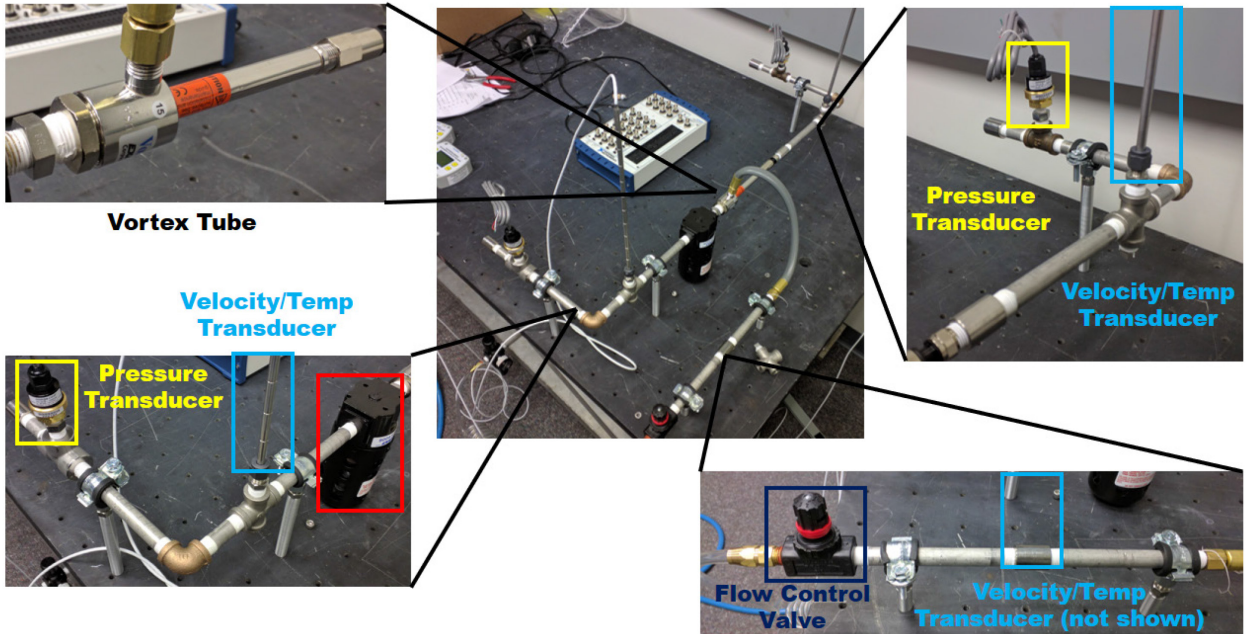


Fig. 28. Experimental setup consisting of a vortex tube, DAQ box, and monitoring sensors

The designed experiments consisted of collecting temperature data from the flow at the cold outlet of the vortex tube due to variations of the main parameters. These experiments also determined the needed value of each parameter for the optimal solution. To recall, these parameters were the following: cold fraction, input pressure, and input flow rate, which were all conditioned with the cold fraction valve, a pressure regulator, and a flow control valve, respectively.

Both the medium vortex tube and small vortex tube were tested during this part of the experimental process. However, one of the main goals was cooling uniformity, the medium vortex tube showed too many inconsistencies in the experimental data to be a viable option for the chamber experiments. The medium vortex tube data will not be shown in the following sections; they will only consist of small vortex tube data. Another important note to consider is that no experiments were performed for a flow that had a cold fraction less than 50%. The final

consideration and one of the project goals was minimal mechanical vibrations. It was important to record the acoustical noise of the system to determine a rough estimate of mechanical vibrations that could affect the system. However, the loudest the system became was 77 decibels; this is approximately as loud as a conversation. ASML determined that this was of no harm to the system and it did not need to be monitored; however, the noise was still damped by replacing certain pipes with plastic tubing.

### 9.2.1. Cold fraction variations

For the ranges of cold fraction variations that were designed for experimental investigation on the cold fraction, the temperature data is plotted against time, Fig. 29.

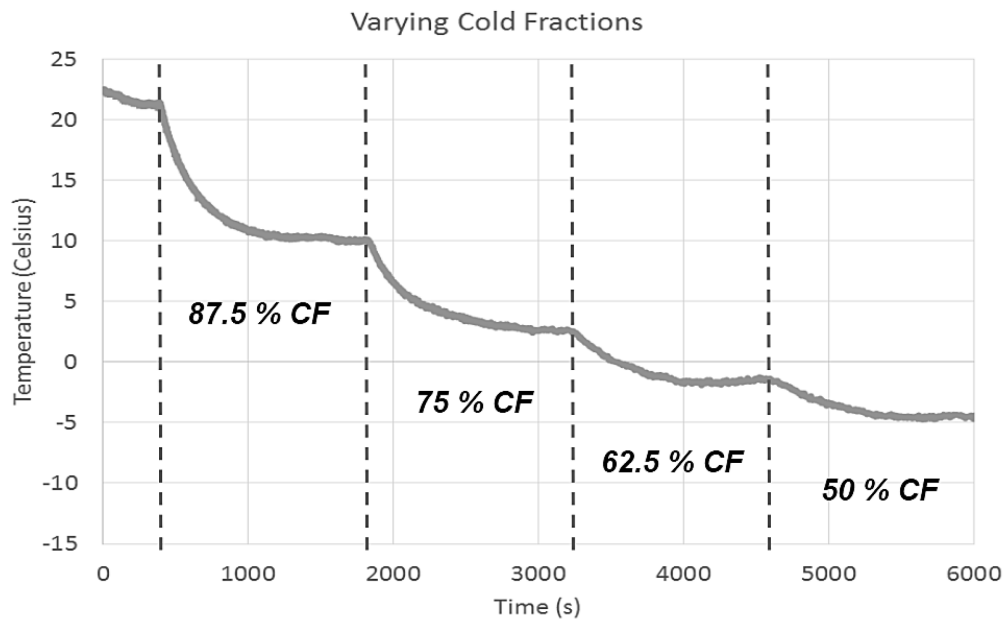


Fig. 29. Cold temperatures plotted over time for varying cold fractions

The plot in Fig. 29 shows that for lower cold fractions, a maximum cooling capacity is achievable by the vortex tube. The coldest temperature achievable, while using more than half of the supplied pressurized air, is approximately  $-5\text{ }^{\circ}\text{C}$ . However, only 50% of the inlet mass flow would be at this temperature, the remaining mass flow would be exhausted into the atmosphere. It is imperative to find the best balance between cold outlet mass flow and air temperature. According to the theoretical analysis, the desirable air temperature needed is  $14\text{ }^{\circ}\text{C}$ . This was achievable at the necessary mass flow at approximately 90% cold fraction. This cold fraction was used in the chamber experiments. Despite the cold fraction, the thermal time constants investigation for the vortex tube average 10-15 min for a one-step process, which is the action of varying a parameter once from a certain value to another.

### 9.2.2. Input pressure variations

Temperature data collected for varying input pressures is plotted over time, Fig. 30.

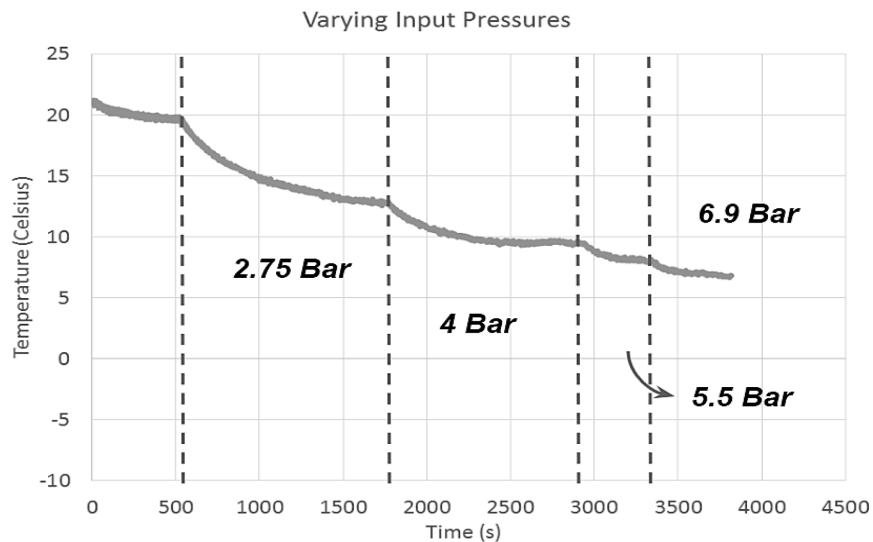


Fig. 30. Cold temperatures plotted over time for varying input pressures

The plot in Fig. 30 shows that the vortex tube operates at maximum capacities for higher pressures, mostly within the 5.5-6.9 bar (80-100 psi) range since the temperature difference at steady state between the two is relatively small. It was determined that 5.5 bar (80 psi) would be a better solution for the system. The lab was limited with air pressure constraints; it had a wall outlet that provided pressurized air at a range of 7.6-9.0 bar (110-130 psi). Due to the performance charts of the control valve that regulated the inlet mass flow, there was a pressure drop through the control valve that needed to be accounted for. This pressure drop was proportional to the inlet air pressure; the higher the pressure, the larger the pressure drop. It was determined that the pressure drop was too great if the pressure from the wall outlet varied too much during experimentation. Because the temperature differential between steady state of 5.5 bar (80 psi) and 6.9 bar (100 psi) is small, 80 psi was a more viable option.

The thermal time constant results for input pressure changes average roughly 10 min, which is a lower response time than that from cold fraction changes. However, these thermal time constants are not even distributed throughout the pressure ranges. Considering the ranges of temperature, the vortex tube will be working with for the cooling of the chamber, the changes in input pressure will provide larger thermal time constants, and thus, cold fraction changes take less time for this application.

### **9.2.3. Reduction of overall thermal time constants**

Noticing from Fig. 29, Section 9.2.1, that a larger cold fraction change generates a higher downslope for the temperature data plotted over time, a two-step process experiment was designed and conducted. This experiment investigated the use of a low cold fraction to force the cold outlet flow temperature to decrease until reaching a desired final temperature, for which the

cold fraction that would produce a flow at the desired final temperature at steady state is then set. This is called the “forced experiment”, where the thermal time constant is reduced.

The data from Fig. 29, Section 9.2.1, is used for interpolation, and a series of final temperatures are determined for any cold fraction. With this, if the final desired temperature is 14 °C, a cold fraction of approximately 90% is required. A simple one-step process for a change of 100% to 90% would produce the normal average thermal time constant, which is 10-15 min, however, with the use of a lower cold fraction, such as 50%, the time is reduced. The two-step procedure involved switching the cold fraction from 100% to 50%, and after the cold outlet temperature approaches 14 °C, the cold fraction is adjusted to 90%, Fig. 31.

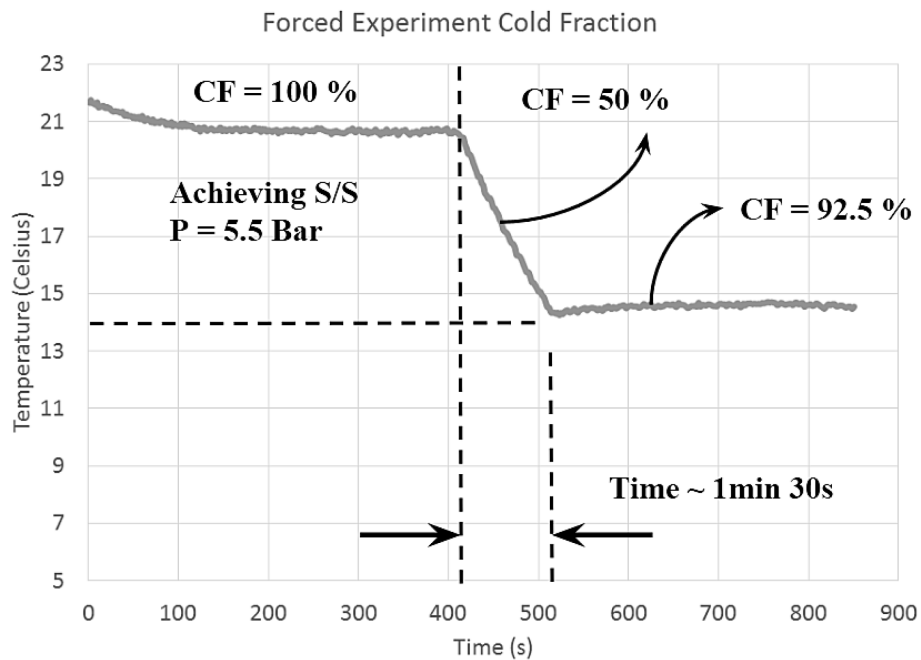


Fig. 31. Cold temperatures plotted over time for the forced experiment

The thermal time constants from the vortex tube for the required application were reduced from 10-15 min to approximately 1 min and 30 sec. Another concern our sponsor had

was after cooling, if we could get the stream temperature back up to ambient temperature quickly. When the heating process was done, they did not want cold air to over cool the plate that was being heated. To mitigate this, investigations were made by using the hot exhausted air and mixing it with the cold air stream. This experiment was tested at various cold fractions, however, due to insufficient mass flow from the hot exhaust, the stream was unable to be reheated. Further conclusions about this will be discussed in future work and recommendations.

### **9.3. Experimental results from forced convection cooling of a heated plate**

Following the designed experimental procedure, Section 7.3, the plate was heated to steady state with the use of the flexible plate heater. At this moment, the vortex tube was connected to the nozzle, allowing it to take in the flow and generate a thin film of cooling flow over the plate, thus, forcing convective cooling. Temperature distributions and magnitudes were monitored for data analysis with an IR camera, as well as strategically-placed thermocouples. Five thermocouples were placed throughout the plate surface; two on the left, and three on the right, Fig. 32. Instead of placing six, one was removed. This is because the thermocouple wire diameters are roughly the same size as the thickness of the flow film being generated by the nozzle outlet. Thus, the fluid interaction with the thermocouples could have potentially caused damage to the transferring of the heat. For referencing, the thermocouples are numbered from 1-5, seen in Fig. 32.

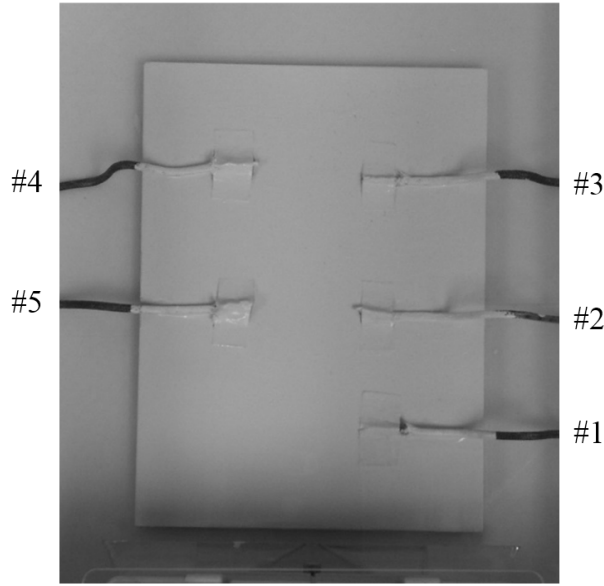


Fig. 32. Thermocouple placements throughout the plate

Additionally, since the IR camera was going to be used to generate thermal imaging of temperature distributions throughout the plate surface, white paint was applied on top of both the ceramic surface and the thermocouples, seen also in Fig. 32. This is because, since the thermocouples have a different emissivity than the ceramic plate, the white paint would provide better uniformity for a better quality of recorded data. The infrared camera was mounted on a high-stability tripod to place the camera in a vertical position on top of the plate, Fig. 33. Due to the low emissivity of acrylic, the cover plate was taken off for these experiments.

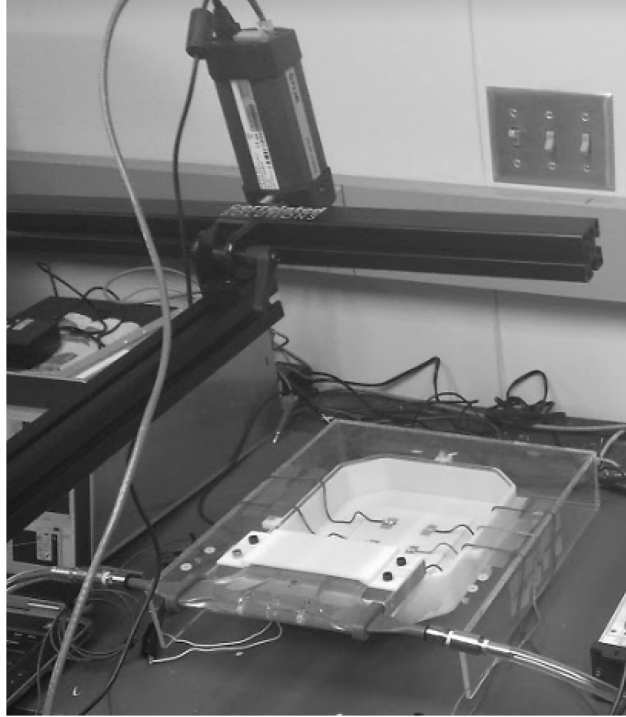


Fig. 33. Positioning for infrared camera to capture area of interest

### **9.3.1. Temperature distributions from IR thermal imaging**

Thermal imaging with the IR camera was recorded, Fig. 34, for two key moments, one of which is when the heating reached steady state, and the other is after connecting the vortex tube to the nozzle and cooling the plate. The coloring scale used for the thermal images was “rainbow”. From the perspective of these images, the nozzle is exhausting flow from the bottom.

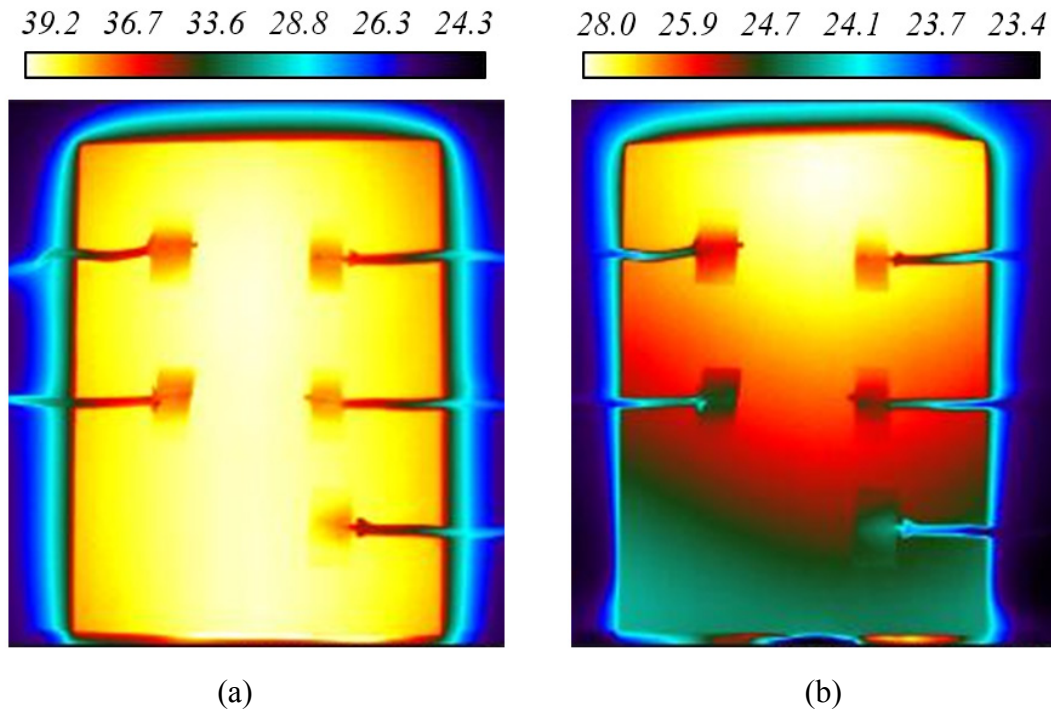


Fig. 34. Thermal imaging of forced convection from IR camera

Evenly distributed heat is clearly noticeable in Fig. 34 (a), however, this is not the case on the outer borders of the plate. This is because the flexible plate heater, being a commercial part, and not custom-manufactured for this application, is smaller in size than the ceramic plate. After cooling, Fig. 34 (b), a clear temperature distribution is seen throughout the length of the plate that is along the direction of the flow. Although this is a general heat convection of flow over parallel flat plates, the distribution is unique. The temperature contour lines would normally be horizontal, but due to the nozzle outlet the lines are parabolic. Keep in mind, since the nozzle contains two inlets, the flow is previously divided in two streams. In the nozzle, each channel is expanded at the outlet, and thus, the flows overlap at the middle and reduce velocity, which in turn, reduces the convective heat transfer coefficient; hence, better cooling at the sides.

The main takeaway here is the fact that the distributions mark a relatively large temperature differential throughout the surface of the plate. Achieving uniform temperature distributions throughout the plate is a critical goal for this project, however, due to time constraints, this could not be completed. A solution for this, however, was designed and included for future development in Chapter 11. There are three major regions marked on the thermal images, the first of includes temperature differentials from 24 to 25 °C, the second from 25 to 26.2 °C, and the third from 26.2 to 28 °C. However, the total temperature differential is approximately 4 °C.

Also noticeable in Fig. 34 (b) is the fact that there is better cooling on the left side in comparison to the right. This is due to the flow's interaction with the thermocouple wires. By removing the first thermocouple at the left, the parabolic temperature contour lines are skewed to the right. Therefore, the flows interaction with the wires damages the amount of heat transfer, rather than improving. The reason that an improvement could have been a possibility is that, if rather than slowing the flow down, the interaction could have solely added turbulence to the flow, which could have resulted with an improved heat transfer. This was not the case, however.

### **9.3.2. Thermocouple temperature data plotted over time**

The temperature data for thermocouples 1-5 were plotted over time from the point before heating until after reaching steady state in cooling, Fig. 35. The plot clearly shows that cooling per surface area decreased throughout the length of the plate.

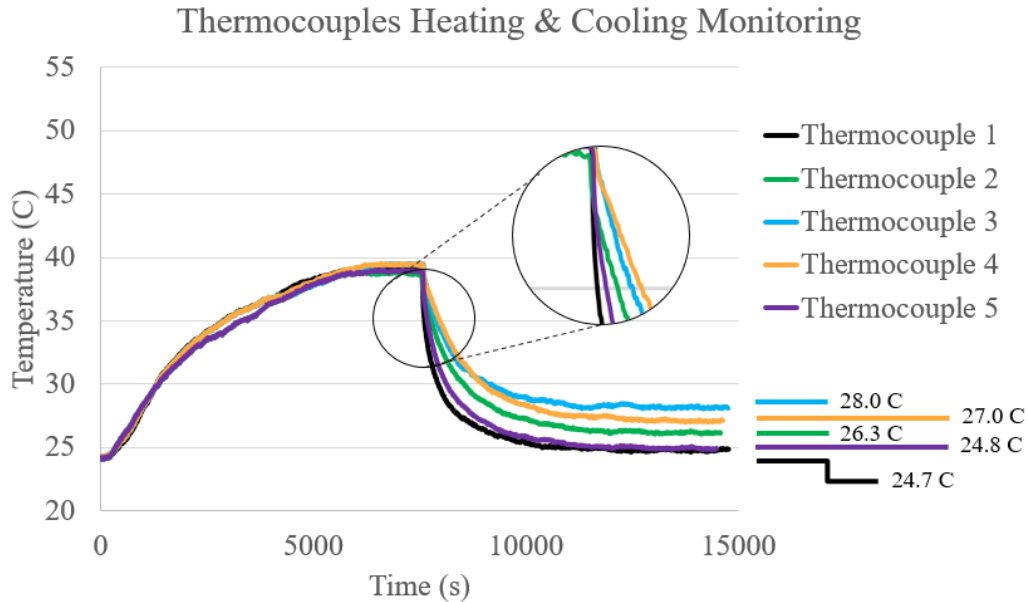


Fig. 35. Temperature data for all thermocouples during heating and cooling experiments

The plot in Fig. 35 shows that, from thermocouples 1-3 the final surface temperature after being cooled to steady state increases. However, following from the key observations made at the thermal images, the thermocouples at the left record lower final temperatures than the right ones. Specifically, at thermocouple 2 the final temperature was roughly 24.8 °C, while thermocouple 2 recorded 26.3 °C. Thus, from the comparison between the middle thermocouples, 2 and 4, a 1.5 °C of difference is determined, which is significant. Interestingly enough, the final temperature of 24.8 °C recorded by thermocouple 2 is 0.1 °C higher than thermocouple 1, which is the closest thermocouple to the nozzle. Additionally, a curious observation from the cooling at the farthest thermocouples, 3 and 4, marks that thermocouple 4 is being cooled at a faster rate than thermocouple 3, however, its final temperature is higher.

Since the first thermocouple had the most interaction with the fluid flow, its temperature data was used for investigation and comparison purposes, Fig. 36.

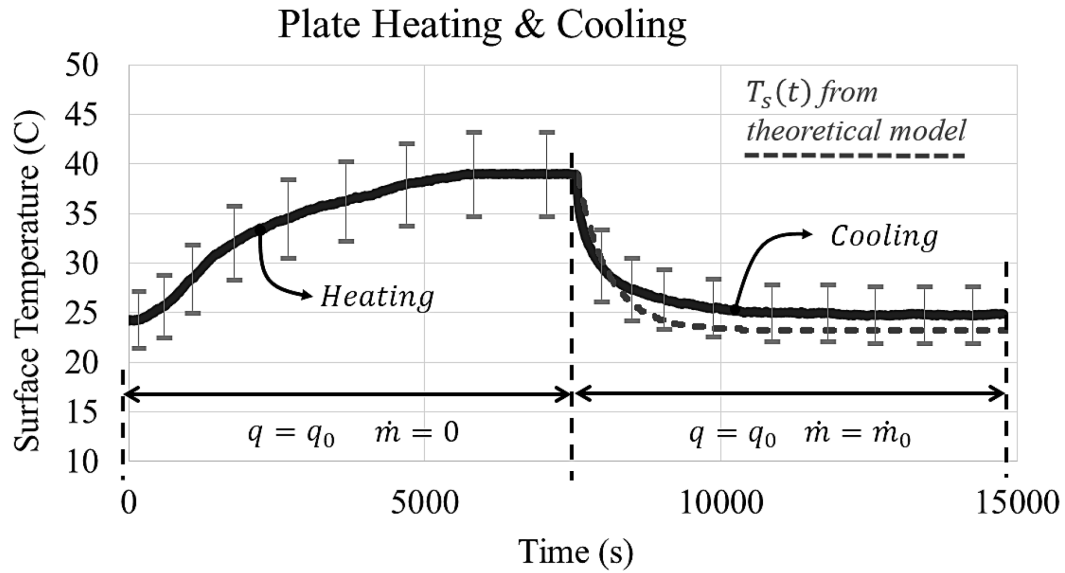


Fig. 36. Temperature data from the first thermocouple plotter over time

The plate reached 39 °C at steady state heating, and was cooled down by the vortex tube flow to an approximate average of 24.7 °C. For comparison purposes, Eq. 4.7, Section 4.2.2, was plotted on the same graph as the experimental data. The comparisons show similarity between the two, however, with an offset of 1 °C. The theoretical model is well within the error margins of the experimental data, nevertheless, which are 10%. The 10% error bars were calculated based on two main portions: the standard error and uncertainties in the experimental setup.

The thermal time constant calculated from the cooling of the flow over the heated plate is approximately 50 min. This is relatively large, however, not of concern. In the photolithography processes, the purpose is to dissipate the amount of heat, rather than cool an already heated plate. Thus, in the application, when the plate is being heated and reaches 23 °C, the vortex tube flow is connected and exhausted in order to dissipate the heat and avoid the plate from reaching high temperatures.

## **10. Conclusions**

The purpose of this project was to determine the viability of using a vortex tube for thermal management in ASML's industrial photolithography machines. The results generated by the project work indicate that the vortex tube is a viable technology for this application. The vortex tube was able to dissipate the required 5 Watts of heat, which lowered the temperature in the experimental environment to ambient temperature (22-24 °C). Additionally, the vortex tube fits the clean room requirements that are necessarily imposed on its use. The vortex tube was able to maintain a specified temperature in the chamber, and was able to cool the chamber to this desired temperature quickly and reliably. Due to these positive results, ASML is looking to continue research in this area in partnership with WPI.

### **10.1. Experimental results of a vortex tube's capabilities and limits**

The experiments conducted to characterize the vortex tube's real life behavior and discover its limits revealed the actual usability of this technology in this particular application. From this, the team was able to eliminate the medium size of the vortex tube technology as a viable option due to its inability to provide consistent cooling uniformity. Therefore, the small vortex tube, which provided a smaller flow rate to the system, was picked as the most optimal technology for this application. This was not without its drawbacks, as the smaller vortex tube would need to be optimized in future work.

### **10.2. Reduction of overall thermal time constants**

The experiments conducted to identify the lowest achievable thermal time constant provided insight into how fast the vortex tube's adjustability was. The original process developed

for experiment involved allowing the vortex tube to reach steady-state at a certain set of parameters, and then allowing it to run until it reached a steady-state temperature to understand its cooling capabilities in that particular experimental range. This provided a much longer time constant than desired. Using the one-step process described above often lead to a thermal time constant of 10 to 15 minutes.

The two-step process used involved the vortex tube's parameters to quicken the thermal time constant of the system. With the two-step process, the vortex tube would reach steady-state at a certain set of parameters, and then one parameter would be adjusted to see how quickly the vortex tube would then cool. The optimal thermal time constant from these two-step process experiments was 1 minute and 30 seconds to reach the desired temperature, which was a marked improvement over the original one-step processes. Therefore, the vortex tube was proved to have the adjustability that ASML desires for a potential cooling system.

### **10.3. Experimental results from forced convection cooling of a heated plate**

With the vortex tube characterized and the optimal setup found, the vortex tube was then attached to a chamber that replicated the environment in which the technology would be applied. From this, the ability of the vortex tube to cool the required amount of heat power was tested. Although not all requirements were met, specifically in terms of the uniformity of the cooling over the plate, the vortex tube was able to dissipate the 5 W of heat generated. This shows that despite the vortex tube needing some adjustment to perform optimally in this system, that it was viable for ASML's needs and is worth exploring its full capacity for thermal management.

#### **10.4. Temperature distributions from IR thermal imaging**

In order to fully visualize and understand the uniformity provided from the small vortex tube, IR thermal imaging was used. This thermal imaging provided visualization for the heat dissipation over the plate. From it, understanding was gained about how effective the vortex tubed based system was in terms of providing fine temperature uniformity over the plate. This lead to the conclusion that the setup used in this set of experiments, which included the small vortex tube connected to a single nozzle, was not currently sufficient to fully stabilize the temperature of the plate at the uniformity required by ASML. Therefore, recommendations were developed in order to make this more effective.

#### **10.5. Thermocouple temperature data plotted over time**

Five surface thermocouples were used to read the temperature on the surface of the plate. These did provide accurate readings; however, due to the thickness of their wiring, they inhibited the flow from the nozzle. The thermocouple thickness affected the cooling ability of the vortex tube overall, and is something that needs to be revised in future testing. The readings attained from the thermocouples helped characterize the uniformity of the temperature over the plate as the vortex tube ran. From it, conclusions were drawn about how the vortex tube was able to cool. It did show that it was capable of cooling to the desired temperature, but there are some limitations with the setup used for this project, and the future work conducted on this should take this iteration and improve it to make the system even more effective than it was.

## 11. Future work and recommendations

Since this project will continue to be worked on in the future, there are further improvements that can be made. Currently, the vortex tube does not provide optimal temperature uniformity along the heating plate. This is likely due to the project using a smaller capacity vortex tube, which may not be able to provide a large enough volume of airflow by itself. A possible solution to this would be to add another nozzle to add crossflow to the plate, and increase the cooling airflow volume.

Another improvement that can be made is to automate more of the system controls. The current system developed in this project relied on human operators to control the valve in the system. Automating these valves would lower the thermal time constant, and should be explored as an avenue of improvement in the next iteration.

Future work also includes investigations regarding structural vibrations generated by the vortex tube. Due to time limitations, these were not explored. Since the vortex tube flow is turbulent, it does generate some vibrations in the system, though these vibration patterns have not been quantitatively identified. Future experiments should be run to identify and understand exactly how structural vibrations may affect the testing environment, and how this effect can be minimized and compensated for in the system design.

Finally, ASML would like to investigate the possibility of mixing the hot and cold outlet of the vortex tube to help regulate temperature in the chamber in between manufacturing runs. The team has developed a preliminary design of this system, which includes automated control valves to regulate the flow from each of these outlets and into the chamber. This system will need proper design, testing, and validation to determine its viability and usefulness as part of this project.

## References

- Bergman, T. L., Lavine, A. S., Incropera, F. P., and Dewitt, D.P. (2011) *Fundamentals of Heat and Mass Transfer*, John Wiley & Sons, Inc, pp. 287-294.
- Blevins, R. D. (1977) "Flow-induced vibration", *Van Nostrand Reinhold Co.*, New York, NY.
- Cengel, Y.A., Cimbala, J.M. (2014) *Fluid Mechanics: Fundamentals and Applications*, McGraw-Hill.
- Deissler, R. G., and M. Perlmutter (1960) "Analysis of the flow and energy separation in a turbulent vortex", *Int. J. Heat and Mass Transfer*, 1(2):173-191.
- Hilsch, R. (1947) "The use of the expansion of gases in a centrifugal field as cooling process", *Review of Scientific Instruments*, 18(2):108-113.
- Kurosaka, M. (1982) "Acoustic streaming in swirling flow and the Ranque-Hilsch/vortex-tube/effect", *J. Fluid Mechanics*, 124:139-172.
- Stephan, K., S. Lin, M. Durst, F. Huang, and D. Seher (1983) "An investigation of energy separation in a vortex tube", *Int. J. Heat and Mass Transfer*, 26(3), pp. 341-348.
- Yilmaz, M., M. Kaya, S. Karagoz, and S. Erdogan (2009) "A review on design criteria for vortex tubes", *Heat and mass transfer*, 45(5):613-632.
- "Economical Pressure Transducers with 5Vdc Output" *Omega*, from <http://www.omega.com/Manuals/manualpdf/M4182.pdf>
- "General Purpose Industrial Air Velocity/Temperature Transmitter/Indicator" *Omega*, from <http://www.omega.com/Manuals/manualpdf/M4791.pdf>
- "UG-281: ADXL312 Quick Start User Guide" *Analog Devices, Inc.*, from <http://www.analog.com/media/en/technical-documentation/user-guides/UG-281.pdf>
- EXAIR vortex tube model 3908 manual guide, *EXAIR*, from <http://www.exair.com/en-US/Primary%20Navigation/Products/Vortex%20Tubes%20and%20Spot%20Cooling/Vortex%20Tubes/Pages/Vortex%20Tube.aspx>
- EXAIR vortex tube model 3930 manual guide, *EXAIR*, from <http://www.exair.com/en-US/Primary%20Navigation/Products/Vortex%20Tubes%20and%20Spot%20Cooling/Vortex%20Tubes/Pages/Vortex%20Tube.aspx>
- "Flexible Silicone Rubber Fiberglass Insulated Heaters" *Omega*, from <http://www.omega.com/Manuals/manualpdf/M1250.pdf>

## APPENDIX A. Project schedule in Gantt chart form

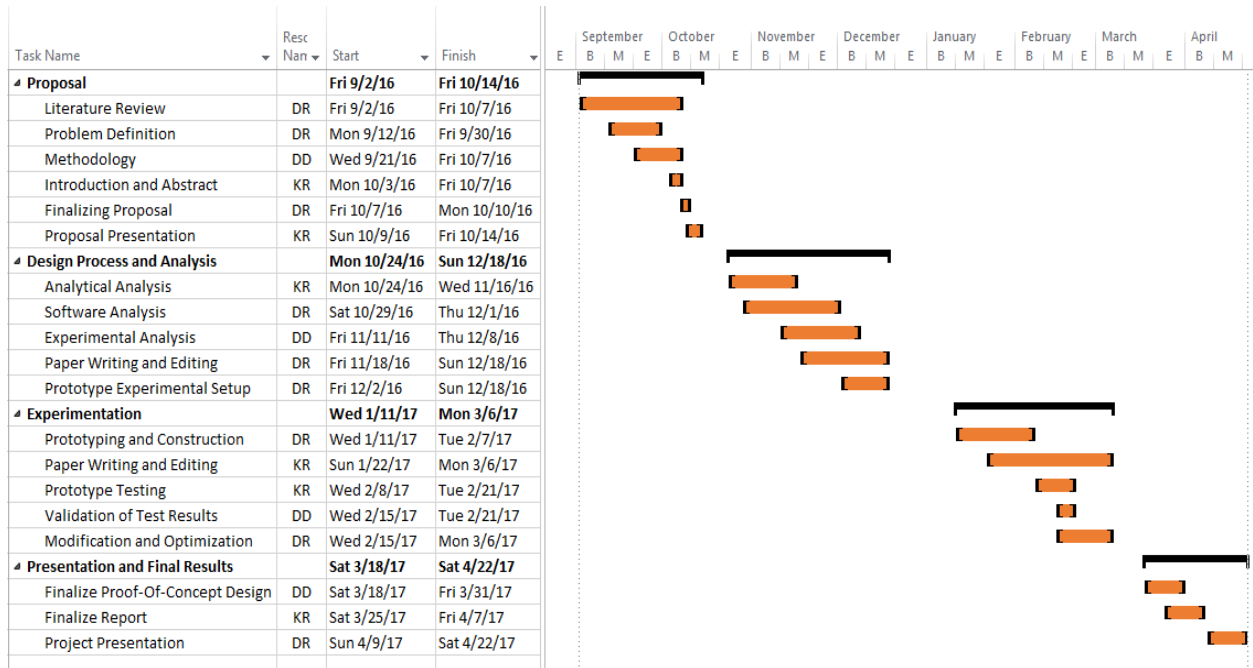


Fig. 37. Project schedule in Gantt chart form

## APPENDIX B. Derivation of some theoretical models

### APPENDIX B.1. Definition for the temperature differential with curve fit functions

$$\begin{aligned}
 CF_{0.2}(p_0) &:= \begin{cases} 0 & \text{if } p_0 \leq 0 \\ \left[ (21.479 \cdot \ln(p_0) - 220.5) \cdot S(1 \cdot 10^5, p_0) - (21.479 \cdot \ln(p_0) - 220.5) \cdot S(8 \cdot 10^5, p_0) \right] & \text{otherwise} \end{cases} \\
 CF_{0.3}(p_0) &:= \begin{cases} 0 & \text{if } p_0 \leq 0 \\ \left[ (20.344 \cdot \ln(p_0) - 208.05) \cdot S(1 \cdot 10^5, p_0) - (20.344 \cdot \ln(p_0) - 208.05) \cdot S(8 \cdot 10^5, p_0) \right] & \text{otherwise} \end{cases} \\
 CF_{0.4}(p_0) &:= \begin{cases} 0 & \text{if } p_0 \leq 0 \\ \left[ (18.88 \cdot \ln(p_0) - 192.81) \cdot S(1 \cdot 10^5, p_0) - (18.88 \cdot \ln(p_0) - 192.81) \cdot S(8 \cdot 10^5, p_0) \right] & \text{otherwise} \end{cases} \\
 CF_{0.5}(p_0) &:= \begin{cases} 0 & \text{if } p_0 \leq 0 \\ \left[ (16.845 \cdot \ln(p_0) - 171.36) \cdot S(1 \cdot 10^5, p_0) - (16.845 \cdot \ln(p_0) - 171.36) \cdot S(8 \cdot 10^5, p_0) \right] & \text{otherwise} \end{cases} \\
 CF_{0.6}(p_0) &:= \begin{cases} 0 & \text{if } p_0 \leq 0 \\ \left[ (14.714 \cdot \ln(p_0) - 150) \cdot S(1 \cdot 10^5, p_0) - (14.714 \cdot \ln(p_0) - 150) \cdot S(8 \cdot 10^5, p_0) \right] & \text{otherwise} \end{cases} \\
 CF_{0.7}(p_0) &:= \begin{cases} 0 & \text{if } p_0 \leq 0 \\ \left[ (12.081 \cdot \ln(p_0) - 123.11) \cdot S(1 \cdot 10^5, p_0) - (12.081 \cdot \ln(p_0) - 123.11) \cdot S(8 \cdot 10^5, p_0) \right] & \text{otherwise} \end{cases} \\
 CF_{0.8}(p_0) &:= \begin{cases} 0 & \text{if } p_0 \leq 0 \\ \left[ (8.9516 \cdot \ln(p_0) - 90.727) \cdot S(1 \cdot 10^5, p_0) - (8.9516 \cdot \ln(p_0) - 90.727) \cdot S(8 \cdot 10^5, p_0) \right] & \text{otherwise} \end{cases}
 \end{aligned}$$

$$\begin{aligned}
 T_{\Delta}(x, p_0) &:= CF_{0.2}(p_0) \cdot S(0.15, x) - CF_{0.2}(p_0) \cdot S(0.25, x) \dots \\
 &\quad + CF_{0.3}(p_0) \cdot S(0.25, x) - CF_{0.3}(p_0) \cdot S(0.35, x) \dots \\
 &\quad + CF_{0.4}(p_0) \cdot S(0.35, x) - CF_{0.4}(p_0) \cdot S(0.45, x) \dots \\
 &\quad + CF_{0.5}(p_0) \cdot S(0.45, x) - CF_{0.5}(p_0) \cdot S(0.55, x) \dots \\
 &\quad + CF_{0.6}(p_0) \cdot S(0.55, x) - CF_{0.6}(p_0) \cdot S(0.65, x) \dots \\
 &\quad + CF_{0.7}(p_0) \cdot S(0.65, x) - CF_{0.7}(p_0) \cdot S(0.75, x) \dots \\
 &\quad + CF_{0.8}(p_0) \cdot S(0.75, x) - CF_{0.8}(p_0) \cdot S(0.85, x)
 \end{aligned}$$

$$T_C(\varepsilon, p_0) := T_0 - T_{\Delta}(\varepsilon, p_0)$$

## APPENDIX B.2. Derivation of velocity distribution function over flat plate

The skin friction coefficient is first substituted in the shear stress equation, and then the shear stress as a function of  $x$  is determined as

$$\tau_w(x) = 0.1\rho v^{1/5} u_\infty^{4/5} x^{-1/5} \quad .$$

The shear stress is then used to define the shear velocity as

$$u^*(x) = 0.316v^{1/10} u_\infty^{4/10} x^{-1/10} \quad .$$

With this, a complete direct function of the velocity with respect to  $x$ , for which the result is

$$u(x) = \frac{0.316 v^{1/10} u_\infty^{4/10} x^{-1/10}}{\kappa} \ln \left( 0.316 y v^{-9/10} u_\infty^{4/10} x^{-1/10} \right) + 0.316 B v^{1/10} u_\infty^{4/10} x^{-1/10} \quad .$$

## APPENDIX C. Detailed steps on modelling turbulence for simulation of flow over plate

### Steps for modelling turbulence simulation of flow over flat plate in COMSOL

Multiphysics are as follows:

1. Identifying the materials for the respective domains: Since the geometry consisted of two domains, the first of which is the chamber cavity and the second is the plate, air and alumina (aluminum oxide) were chosen, respectively.
2. Selecting the physics: “Turbulent Flow,  $k$ - $\epsilon$ ” was the physics used for this simulation. In the settings for the physics, Fig. 38, the physical model for the flow was identified as incompressible. When modelling turbulence, COMSOL will automatically fill some common values for the turbulence model parameters. It is important to specify that the Karman constant,  $\kappa_v$ , is 0.41 and the arbitrary constant,  $B$ , is 5.2. These values must be specified in Eq. 4.3 from the theoretical development of the log law.

The image shows a screenshot of the COMSOL Multiphysics software interface. The 'Physical Model' section is expanded, showing the following settings:

- Compressibility: Incompressible flow
- Turbulence model type: RANS
- Turbulence model:  $k$ - $\epsilon$
- Neglect inertial term (Stokes flow)
- Enable porous media domains
- Use shallow channel approximation
- Reference pressure level:  $P_{ref}$  1[atm] Pa

The 'Turbulence Model Parameters' section is also expanded, showing the following values:

Parameter	Value	Unit
$C_{\epsilon 1}$	1.44	1
$C_{\epsilon 2}$	1.92	1
$C_{\mu}$	0.09	1
$\sigma_k$	1	1
$\sigma_{\epsilon}$	1.3	1
$\kappa_v$	0.41	1
$B$	5.2	1

Fig. 38. Turbulent flow,  $k$ - $\epsilon$  physics settings in COMSOL

3. Setting up initial and boundary conditions: Initial conditions were specified for the air in the chamber cavity before the nozzle exhausts the cooling air. At this moment, the air is assumed to be completely still, thus, the velocity field for X and Y were specified as 0, as well as the pressure as 1 atm. Boundary conditions were named in the tree manager as wall conditions. Since this simulation is solely for fluid mechanics purposes, all walls, excluding the inlet and outlet, were chosen as adiabatic, Fig. 39. COMSOL will automatically consider the walls as adiabatic if no heat transfer physics is added. The wall functions option was chosen as the boundary condition at the walls, which is very common in modelling turbulence.



Fig. 39. Boundary conditions chosen as wall functions (blue lines) in COMSOL

4. Identifying the inlet and outlet boundaries: Velocity was chosen as the boundary condition for the inlet at the nozzle. Since relative uniformity is assumed in the flow, a normal inflow velocity of 9 m/s was specified. Turbulence conditions must also be stated. For simplicity, the turbulent length scale and intensity options were used for defining the conditions, for which the intensity was left as the common value provided by COMSOL, and the length scale was assumed to be 50% of the nozzle outlet width. In other words, 50% of turbulence is assumed in the flow. The outlet boundary conditions were defined

regarding the pressure. The pressure at the outlet was specified as 1 atm, and the option “Normal flow” was selected.

5. Generate mesh: A mesh was generated for the air domain, Fig. 40. For simplicity, the sequence type for node positioning was specified as a physics-controlled mesh. This type of mesh will generate finer element sizes as the nodes approach the walls. This is critical for accurate velocity profiles with vertical distance and boundary layer thickness distributions results. A “coarser” option for the element size was chosen.

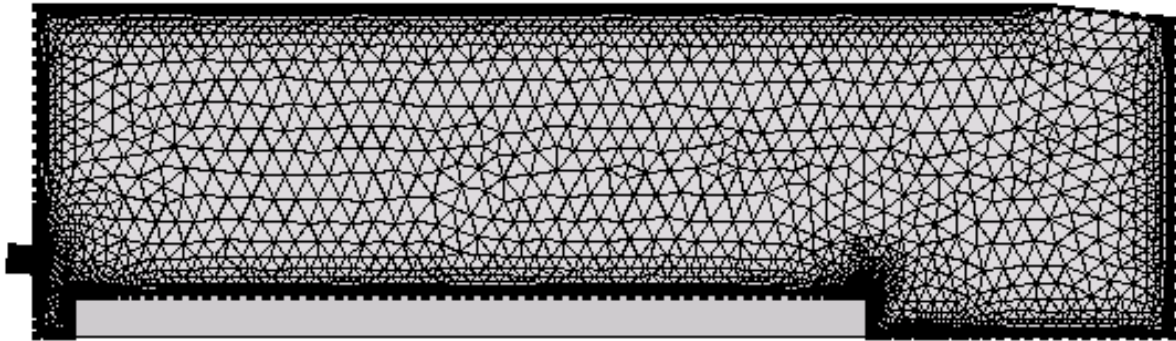


Fig. 40. Generated mesh of the air domain in COMSOL

6. Generate solution for the study: For this simulation, a stationary, rather than transient, solution was computed.

## **APPENDIX D. LabVIEW VI data acquisition coding**

The final VI that was developed consisted of a module to read the analog output signals of the sensors in the experimental setup. It converted these voltage signals into readable parameter values, a timing module, and any other conversions or offsets that were developed through calibration of the setup, as well as a method to allow the data to be written to a Microsoft Excel spreadsheet for analytical review after an experiment was performed. While this program is not complex, it served its purpose and allowed for accurate, repeatable data acquisition. The number of sensors used as well as their power requirements made it not possible to power the sensors solely using the DAQ's power supply. Therefore, separate DC power supplies were used to power these sensors. These separate power supplies allowed for the VI to be less cluttered and left less room for potential programming errors in the duration of the project.

There are two main modules that control the signals from the DAQ. The first module controls the thermocouple. The thermocouple module connects to the physical channel where the thermocouple is powered. The settings for the thermocouple used are input on the front panel. The maximum and minimum read temperature was set based on the specification of the thermocouple. The thermocouple is then connected to a read function. The case structure containing this module can be seen in Fig. 41.

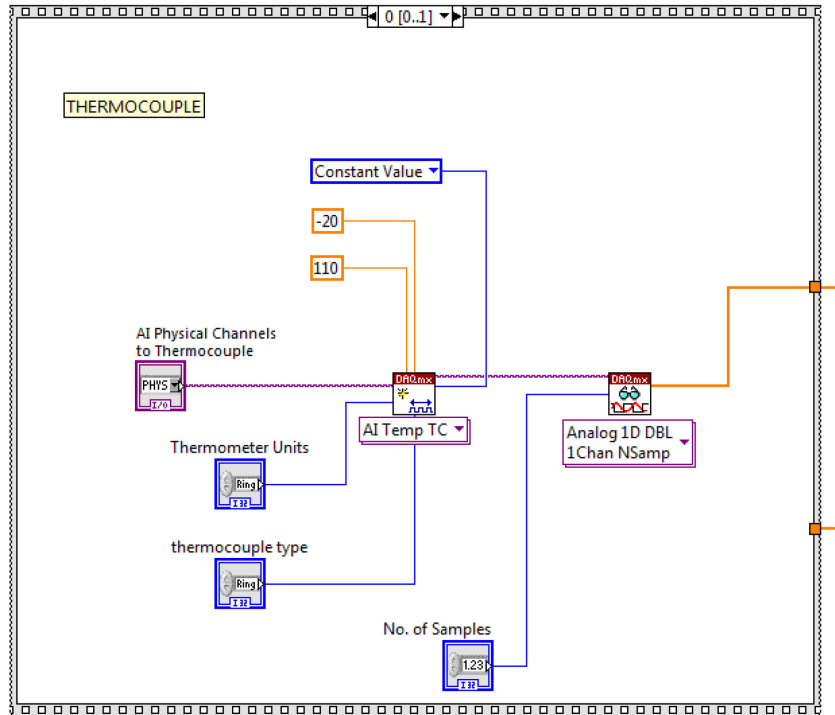


Fig. 41. LabVIEW thermocouple read function

The second function that controls the data coming from the DAQ is the Analog Input function. This function is responsible for reading all of the sensors that output a Vdc signal. From this, a minimum/maximum voltage was assigned based on the sensor's specifications, as well as a module to regulate the specific channels that are read when the VI is running. From this analog input module, the data is sent to a read function, which produces a single stream of data that consists of all of the sensor readings from the VI. This function can be seen in Fig. 42.

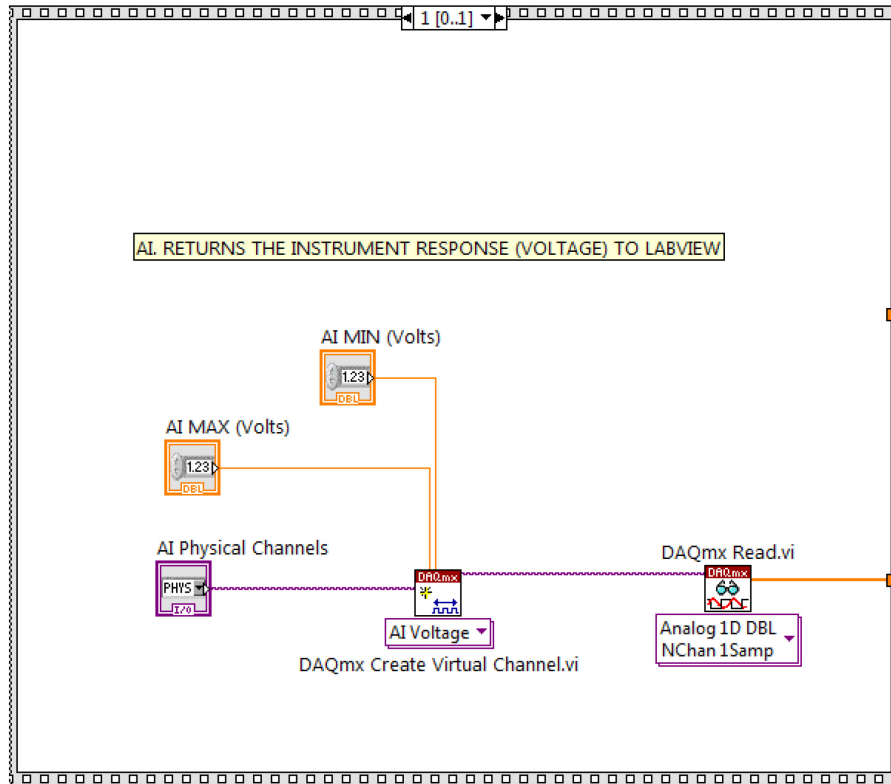


Fig. 42. LabVIEW analog input read function

The two data streams from this case structure are sent to separate parts of the block diagram. The thermocouple data stream gets sent directly into a module to convert the voltage that the thermocouple outputs into a temperature reading. This module begins with a temperature averaging function that took the readings from the thermocouple to find a mean reading. This average is then sent into a slope-intercept equation to convert the thermocouple reading into a temperature reading. The temperature can then be observed using a waveform chart. The process of converting the thermocouple voltage can be seen in Fig. 43.

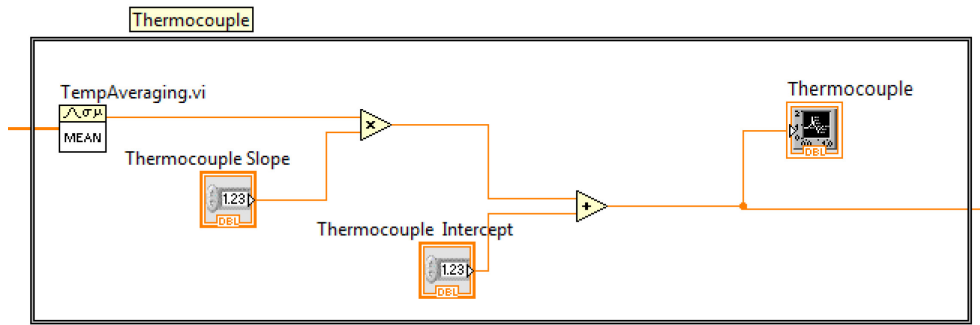


Fig. 43. LabVIEW thermocouple conversion

The data stream from the analog inputs is then sent into an array function, Fig. 44, that splits the data the analog input module receives into separate streams for each individual port on the DAQ. This allows for the VI to produce visible readings for each sensor.

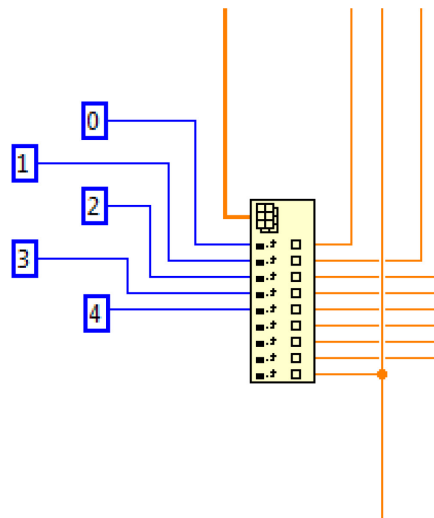


Fig. 44. LabVIEW array function for sensor data

For each individual sensor used to report data, there is a waveform chart on the Front Panel of the VI that can be viewed while the program is running. The waveform chart provided an opportunity for the stability of the reading to be viewed; the signal could be seen in a physical format that could check the range. The individual sensor information is converted from

the voltage signal the sensor produces into a readable parameter, and is sent to a waveform chart, Fig. 45.

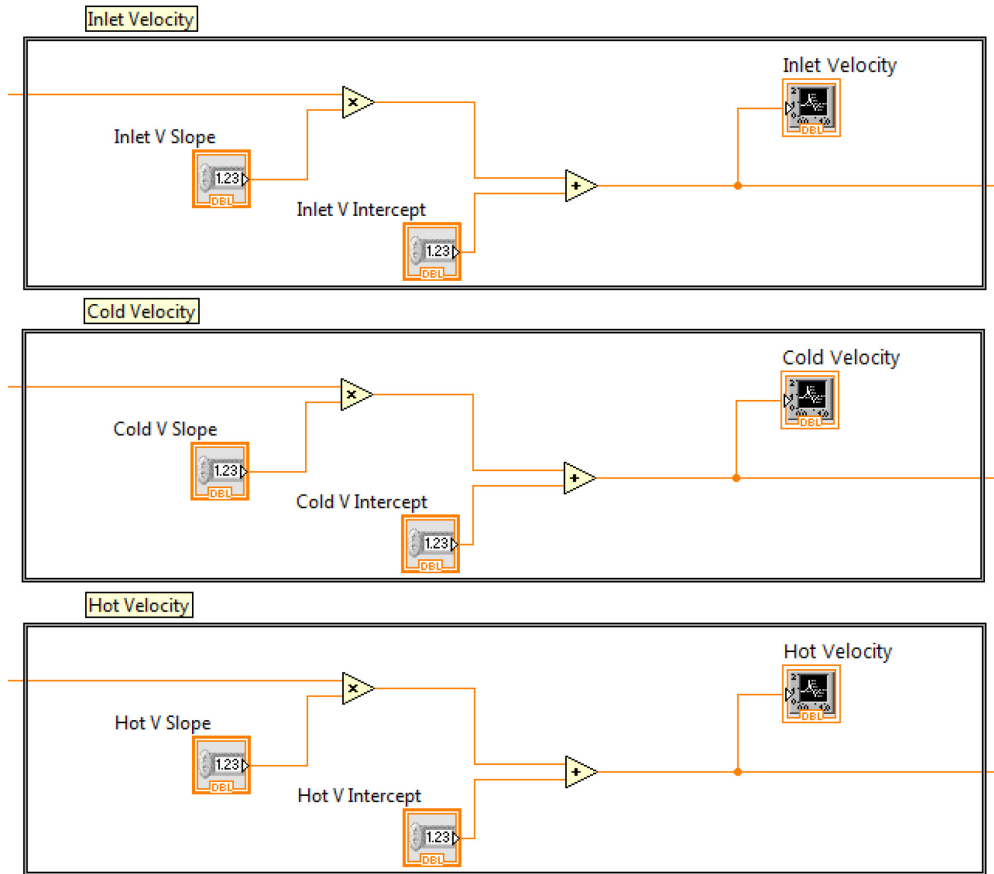


Fig. 45. LabVIEW velocity readings

The timing module, Fig. 46, reads the time that has elapsed during the experiment and can be viewed from the DAQ. The timing module was used because the thermal time constant of the experiments performed was an essential part of our project.

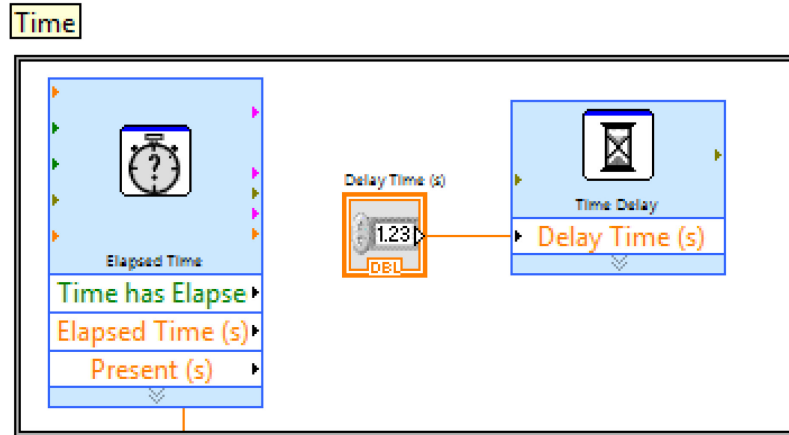


Fig. 46. LabVIEW timing module

The final module, before the separate sensor readings are sent to the build array, is used to convert the velocity readings from each of the sensors into mass flow rate readings. The transducers used for these experiments output a voltage for air velocity, but the desired parameter for these experiments for verification is the mass flow rate. Therefore, all three of the sensors that read velocity must be converted before being recorded for data analysis. The module takes the area of the inner diameter of the piping, multiplies it by the density of the air used, and then multiplies this constant by the velocity reading from the sensor.

To input all of the data into an Excel file, the separate data streams from each of the sensors are put into a build array, which converts them all into a single stream that can be sent to a write to file module. The write-to-spreadsheet module takes the data recorded and allows it to be written as an MS Excel (.xls) spreadsheet. This particular function can also control the decimal place of the data recorded. This module is fairly straightforward, and can be seen in Fig. 47.

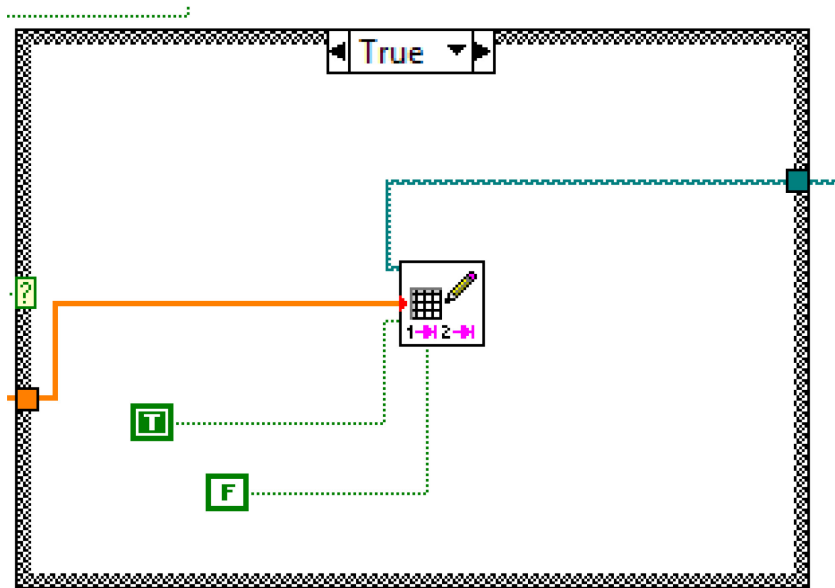


Fig. 47. LabVIEW write-to-spreadsheet function

All of the above programming takes place in a while loop that allows for each of the functions to be repeated continuously until a stop switch on the front panel is activated. This allows for a constant stream of data throughout the entire experiment. The only function that takes place outside of the while loop is a concatenate string function which writes the titles of each data column in the spreadsheet.

**APPENDIX E. List of instrumentation and apparatus**

Table 6. Detailed list of instrumentation and apparatus

<b>Description</b>	<b>Part number</b>	<b>Vendor</b>	<b>Quant.</b>
<b>Conditioning Instrumentation</b>			
Air Accumulator	S/N C109348	SPEEDAIRE	1
Space-saver stacked air filter/regulator	4910K82	McMaster-Carr	2
DC Power Supply 0-100V .2 A	9184	BK PRECISION	1
Data Acquisition Box	NI USB-6229	National Instruments	1
Pneumatic flow control valve	6ZC08	Grainger	1
<b>Monitoring Instrumentation</b>			
Pressure transducer	PX181B-100G5V	OMEGA Engineering	3
Air velocity/temperature RTD transmitter	FMA1003R-V1	OMEGA Engineering	3
Threaded thermocouple probe	1245N19	McMaster-Carr	1
Pressure gauge	4003K713	McMaster-Carr	1
3-axis MEMS accelerometer, range +/- 1.5g	EVAL-ADXL312Z-ND	DigiKey Electronics	1
Surface type-T thermocouple	9251T96	McMaster-Carr	5
<b>Environment Replicating Instrumentation</b>			
EXAIR 3204 vortex tube cooling kit	3908	EXAIR	1
EXAIR 3215 vortex tube cooling kit	3930	EXAIR	1
3D printed components	N/A	N/A	N/A
Flexible heater silicon rubber	SRFG-406/2	OMEGA Engineering	1
Alumina ceramic sheet, 157x117x5mm	Custom order	Precision Ceramics	1
Infrared Camera	SC600 Series	FLIR	1